Heliophysics Senior Review 2010

The Reuven Ramaty
High Energy Solar Spectroscopic Imager
(RHESSI)

Robert Lin, Principal Investigator

Brian Dennis, Mission Scientist

Manfred Bester, Mission Operations Manager

Laura Peticolas, E/PO Manager

Table of Contents

1 EXECUTIVE SUMMARY

The RHESSI Small Explorer mission is designed to investigate particle acceleration and energy release in solar flares through imaging and spectroscopy of hard X-ray (HXR)/gamma-ray continua emitted by energetic electrons, and of gamma-ray lines produced by energetic ions. The single RHESSI instrument provides ground-breaking imaging and spectroscopy measurements over the broad energy range from soft X-rays (3 keV) to gamma-rays (17 MeV). RHESSI was launched in February 2002, and has been operating successfully ever since. Over 50,000 events are included in the RHESSI Flare List, 11,000 of them with detectable emission identified above 12 keV, ~950 above 25 keV, and 30 above 300 keV with 29 showing gamma-ray line emission. In addition over 25,000 microflares have been detected above 6 keV. Since the start of the mission, all the data and the analysis software have been made immediately available to the scientific community.

RHESSI provides unique observations of high-energy processes close to the Sun that address the key goals of the Heliophysics Great Observatory: understanding the fundamental processes of particle acceleration and energy release in solar eruptions, both flares and CMEs. The resulting photon emissions and accelerated particles directly affect our Home in Space, and are especially important for our Journey Outward.

In the ~2 years since the last Senior Review, analysis of RHESSI observations has resulted in over 200 publications (see: http://www.lmsal.com/~aschwand/publications/rhessi.html). Some of the new results include:

- The detection by RHESSI in a limb-occulted flare of a non-thermal coronal HXR source that is consistent with the coronal energy release/acceleration region predicted by the Drake et al (2006) theory/simulations of a magnetic reconnection model, where electrons are accelerated by volume-filling magnetic islands and end up with up to ~60% of the magnetic energy. This source contains ~10^{36} electrons above 16 keV in a volume of ~10^{27} cm^3, with energy density comparable to that of the ~30-50 Gauss magnetic field (determined from spectra of the co-spatial microwave source).
- The development of a powerful analysis method for ***imaging spectroscopy***, the production of an "image cube" of HXR intensity (I) versus 2-D position (x, y) and photon energy (ε) from RHESSI's raw data – i.e., temporal modulation of fluxes – using visibilities and iterative algorithms.
- The development of an even more powerful analysis tool that combines the direct spectral inversion of the RHESSI HXR measurements with imaging spectroscopy to obtain maps of the flux spectrum F of the ***parent HXR-producing electrons*** versus (x, y) and electron energy E. Such maps have been constructed for a flare and compared to a theoretical model of electron acceleration by turbulence, thus obtaining the characteristics of the turbulence.
- The simulation of the effects of albedo on the spatial properties of HXR sources, showing that they are enlarged by up to 250%, thus providing a natural explanation for HXR footpoint sources usually being more extended than seen in optical or EUV. Some HXR sources are observed as small as <4", however, suggesting an unusually low source altitude.
- The finding that all RHESSI flares associated with a high energy solar energetic particle (SEP) event show soft-hard-harder (SHH) spectral evolution of the flare HXR burst, while none of the flares with soft-hard-soft (SHS) (normal) evolution are associated with an SEP event, thus confirming the previously found close association of SHH behavior with SEP events. This is puzzling since the HXR emission is dominated by the flare footpoints while high energy SEPs appear to be accelerated by CME shocks high in the corona.
- The first survey of coronal HXR emission, using partially disk-occulted flares, showing that ~90% of the 55 flares have a thermal component plus a higher energy non-thermal component that show rapid variations
- The analysis of explosive chromospheric evaporation in a flare, combining RHESSI HXR observations with Hinode EIS measurements that show downflows of thermal plasmas below 1.8 MK and upflows at higher temperatures.
- The finding that many flares show initially downward motions in coronal X-ray sources and decreasing separation in footpoints (suggesting implosions) before the usual rising coronal sources and increasing separation of footpoints in the main phase of the flare.
- The full simulation of the RHESSI instrument to obtain its response extending to 150 MeV, essential for the analysis of the extremely energetic flares such as January 20, 2005, where pion decay becomes important.
- The identification of a second acceleration phase in the January 20, 2005 flare that resulted in a much harder particle spectrum, and possibly may be related to the SEP acceleration that produced the GLE event detected at

the Earth. Since most of the 2.223 MeV line emission is from this phase, the line source imaged by RHESSI may be due to the SEP acceleration.

- The finding of a very close linear correlation between >0.3 MeV gamma-ray continuum and 2.223 MeV neutron-capture line fluences, extending from the limit of detectability to the most intense flare, indicating that the acceleration of the parent relativistic electrons and >~30 MeV protons must be closely related. Thermal soft X-ray emission and HXR emission above 50 keV are also closely linearly correlated to 2.223 MeV line fluence for the flares with the most intense line fluences, but show large excesses for flares with weaker line emission.
- The first systematic survey of over 25,000 microflares observed in RHESSI's first five years, showing that they are all located in active regions, and that they typically have steep power law components with no discernible low energy cutoff - thus their non-thermal energy content is much higher than expected.
- The determination of stringent upper limits to the quiet Sun HXR emission, that rule out heating of the quiet corona by nanoflares with the same properties as typical flares, and set constraints on axion properties.
- The most precise solar oblateness ($R_{equator} - R_{pole}$) measurement ever made (10.58 ± 0.44 mas), obtained by RHESSI's SAS (Solar Aspect System). This large excess over the oblateness predicted (7.98 mas) for solar rotation disappears if regions with low level emission detected by LASCO/EIT are masked off, indicating that the excess is likely due to low-level faculae spread across the solar disk and not just in the active latitudes.
- The finding that the acceleration profile for fast CMEs is closely synchronized to the associated flare energy release observed by RHESSI.
- The comprehensive studies of Terrestrial Gamma-Ray Flashes (TGFs) observed by RHESSI, providing constraints on TGF altitudes and beaming, and showing that TGFs are associated with intra-cloud lightning.

The spacecraft and instrument continue to operate nominally. Now, two and a half years after RHESSI's germanium detectors were annealed, they are again showing the effects of radiation damage as predicted, including significant loss of active volume in both the front and rear segments. The detectors will be annealed again once solar activity increases significantly, so there is a high probability of the occurrence of large gamma-ray events. Thus, RHESSI is ready for the rise to solar maximum expected in ~2012. Since the mission was designed with no expendables and the orbit decay has been minimal, RHESSI should be able to operate for years to come.

The Large Area Telescope (LAT) and the Gamma-ray Burst Monitor (GBM) on Fermi, launched in June 2008, will provide complementary X-ray and gamma-ray spectroscopy of large solar flares extending to energies as high as several hundred GeV, well above RHESSI's highest energy of 17 MeV. The recent launch of the Solar Dynamics Observatory (SDO) will add full-Sun, high-cadence, multi-wavelength imaging and photometry. In addition, Hinode is providing the high cadence measurements in broad–band soft X-rays, diagnostic EUV spectroscopy, and optical/vector magnetograms required for flare studies. STEREO is providing stereoscopic EUV imaging of flares, coronagraph imaging of CMEs, radio burst tracking, and multi-point in situ measurements of energetic particles and plasma/fields. Thus, for the first time, the elements of the Heliophysics Great Observatory (HGO) required for comprehensive studies of energy release and particle acceleration processes in flares and CMEs will be available, just as solar activity is rising towards maximum.

2 SCIENCE

The past two years have been tremendously productive scientifically for the RHESSI mission. RHESSI has provided (and continues to provide) an enormously rich data set. A detailed description of the RHESSI mission, instrument, and software is given in the first six papers of the Nov. 2002 issue of Solar Physics (vol. 210, p. 3-124). Here is a brief summary.

RHESSI provides high-resolution imaging and spectroscopy of bremsstrahlung X-ray/gamma-ray continuum emitted by energetic electrons, and gamma-ray lines produced by energetic ions. At HXR and gamma-ray energies, the only viable method of obtaining arcsecond-class images within the SMEX constraints is with Fourier-transform imaging. The RHESSI instrument has an imager made up of nine Rotating Modulation Collimators (RMCs), each consisting of a pair of widely separated grids mounted on a rotating spacecraft, to achieve angular resolution as fine as ~2 arcsec and imaging up to gamma-ray energies. Behind each RMC is a segmented germanium detector (GeD) to detect photons from 3 keV to 17 MeV. The GeDs are cooled to ~90 K by a space-qualified long-life mechanical cryocooler to achieve the high spectral resolution (~1 to 10 keV FWHM). The GeDs were successfully annealed in November, 2007, to mitigate radiation damage. They will be annealed again as solar activity increases and the probability of an X-class gamma-ray flare becomes significant again.

As the spacecraft rotates, the RMCs convert the spatial information from the source into temporal modulation of the photon counting rates of the GeDs. Pointing information is provided by the Solar Aspect System (SAS) and redundant Roll Angle Systems (RASs). An automated shutter system allows a wide dynamic range ($>10^7$) of flare intensities, from microflares to the largest X-class flares, to be handled without instrument saturation, and it allows the sensitivity to be maximized when low-energy (<~20 keV) X-ray fluxes are low. The spin-stabilized (~15 rpm) spacecraft is Sun-pointing to within ~0.2º and operates autonomously, with the energy and time of arrival for every photon stored in a solid-state memory (sized to handle the largest flare) and telemetered to the ground.

The RHESSI observations provide powerful diagnostics because: (1) they combine high spatial resolution, high spectral resolution, and excellent precision; (2) they span an enormous energy range from soft X-rays (~3 keV) emitted by hot thermal plasmas, through the hard X-ray/gamma-ray continuum emitted by accelerated electrons, to gamma-ray lines emitted by accelerated ions; (3) data for every detected count are brought to the ground so there is unlimited flexibility in the data analysis; and (4) the X-ray and gamma-ray emission processes are quantitatively well-understood.

Thus, significant effort over the past two years was devoted to developing optimal methods to infer the X-ray/gamma-ray distribution in energy, angle, time, and space from the RHESSI measurements. Recently, a new technique has been developed that utilizes the imaging spectroscopy measurements to go directly to the distribution of the ***parent X-ray-producing electrons*** in energy, angle, time, and space. Methods have also been developed to take into account the effect of albedo – scattering of the photons from the dense photosphere – on the X-ray spectrum. This also allows information on the directivity of the electrons to be inferred, and to correct for it in deriving the parent electron source spectrum

The RHESSI flare observations appear to be generally consistent with the flare electron (and ion) acceleration being intimately related to the magnetic reconnection occurring high in the corona above the flare loops. For many flares the accelerated electrons with tens of keV contain >~10-50% of the total energy released in the flare. Since reconnection ideally results in bulk flows, a long-standing question is, how can the energy released be converted to energetic electrons? In the last few years, this problem has been addressed by leading plasma theorists and simulation experts, and possible explanations have been put forward that arises naturally from the reconnection process (Drake et al 2006; and others) that also appears to explain electron acceleration in a reconnection event observed in situ in the Earth's deep magnetotail. In the past several years there have been systematic searches for relatively weak coronal HXR emission when the flare footpoints are occulted by the limb, and some candidates for the energy release/electron acceleration region have been found.

The present extended solar minimum in the last few years has been ideal for systematic studies of microflares and their implications for coronal heating, and of quiet Sun (no active regions) X-ray emissions, with RHESSI's uniquely high sensitivity from ~3 to 15 keV (with the attenuators out of the field of view).

In addition, RHESSI's Solar Aspect System (SAS) has provided the best solar optical shape measurements (e.g., oblateness) ever obtained, opening up a new area of research. The same data now are providing the best observations of the photospheric temperature structure, a crucial signature of interior meridional flows related to the solar cycle.

Furthermore, RHESSI's discovery that TGFs commonly extend up to >~20 MeV has revitalized the study of lightning related high-energy phenomena, and RHESSI provides unique measurements for astrophysical high-energy phenomena, from cosmic gamma-ray bursts to deep searches for low-mass axions produced in the solar core.

To tap the real power of RHESSI requires the integration of its data with that of the other HP missions. To understand what is special about the flare and CME-related particle acceleration and energy release regions identified by RHESSI, we need good magnetic field models based on accurate vector photospheric (and chromospheric if available) measurements, and information on the magnetic topology, waves, shocks, and ambient conditions in the corona obtained by instruments on Hinode, STEREO, and now SDO, as well as on TRACE, SOHO, and groundbased observatories. Fermi can now provide solar gamma-ray measurements more than an order of magnitude higher in energy than RHESSI. To understand the Sun's connection to the heliosphere will require ACE, Wind, STEREO, SOHO, and other spacecraft measuring energetic particles, radio emission, magnetic fields, and the solar wind. We want to understand what conditions lead to these high-energy eruptive phenomena. Many results (see below) have now appeared in the literature showing the power of such multi-platform comparisons. Now for the first time, we have a full complement of multi-platform solar/heliospheric measurements when solar activity rises towards maximum.

2.1 Accomplishments

To date, there have been over 800 papers and 30 PhD theses published using RHESSI data (see Section 2.3.2). They cover a very wide range of topics, so we are only able to highlight below some of the areas of current research.

2.1.1 Hard X-rays & Parent Electrons

2.1.1.1 New Imaging Spectroscopy Methods

One of the main science goals of RHESSI is ***imaging spectroscopy***, the production of an "image cube" of HXR intensity (I) versus 2-D position (x, y) and photon energy (ε). Knowledge of the cross-section for the hard X-ray emission process then allows us to transform this into the real science goal – a map of the accelerated electron flux spectrum F versus (x, y) and electron energy E. Over the past few years or so, major advances in this transformation have been made.

RHESSI stores imaging information through the temporal modulation of flux by the nine sets of rotating grid pairs. This information is most readily translated into visibilities, two-dimensional spatial Fourier transforms of the image (Hurford et al. 2002, Schmahl et al. 2007). Traditional ways of making hard X-ray images with RHESSI data utilize back-projected 'dirty maps' as input and apply deconvolution algorithms (e.g., Clean, MEM, Pixon) to reduce the blurring effects induced by the Point Spread Functions of the RHESSI collimators. However, imaging information is fundamentally encoded by RHESSI through the temporal modulation of incoming flux rather than by the use of focusing optics. This temporal modulation pattern, the purest form of RHESSI data stream, corresponds to specific set of spatial Fourier components of the source. These (complex) Fourier components are termed *visibilities* and, because of their direct relation to the observed count rate, they have straightforwardly quantifiable uncertainties. Forward-fitting the visibility pattern from a parametrized source structure to the observed visibility values therefore results in best-fit values, with uncertainties, for the source parameters (Xu et al. 2008).

The main challenge in producing non-parametric images from visibilities is the rather sparse sampling of the (u,v) frequency plane by RHESSI's nine collimators. To circumvent this, a new visibility-based imaging method has been introduced by Massone et al (2009). The method, termed *uv_smooth*, utilizes two powerful mathematical tools: (1) an interpolation routine to generate a smooth continuum of visibilities within the disk encompassing the sampled area of the spatial frequency plane; and (2) an iterative algorithm incorporating a constraint that the image flux should be everywhere non-negative. Application of this method drastically reduces the "ringing" effects associated with the sparse frequency-plane sampling and also effectively estimates the values of Fourier components outside the range directly sampled by RHESSI. This interpolation/extrapolation method is a very natural approach to RHESSI imaging, utilizing the data in its purest form. It also generates visibility values at equally-spaced points in the spatial frequency plane, so permitting the use of a Fast Fourier Transform (FFT) routine to provide image reconstructions in a very fast and reliable manner.

The underlying science objective of RHESSI, however, is to obtain a map of the ***parent HXR-producing electron*** flux spectrum F as a function of (x, y) and the ***electron*** energy E. "Traditional" imaging spectroscopy proceeds by "stacking" count-based images (each essentially obtained – as noted above – by performing an inverse spatial Fourier transform) at different ε to produce the hard X-ray spectrum $I_k(\varepsilon)$ in each prominent feature k; established spectral inversion techniques (e.g., Piana et al. 2003), coupled with knowledge of the cross-section for the hard X-ray emission process, may then be used to infer the responsible electron flux spectrum $F_k(E)$ for the feature in question. The main drawback in this approach is in the fact that the counts in different energy ranges are independent statistical quantities, so that feature spectra $I_k(\varepsilon)$ thus inferred are rather noisy. Due to the ill-posed nature of the spectral inversion problem, this noise is in general considerably amplified in the recovered electron spectra $F_k(E)$. As a result, the image cube associated with the emitting electrons will not vary smoothly with energy, as expected physically. This significantly impedes the inference of the underlying physics affecting the spatial variation of F(E).

A powerful new imaging spectroscopy method introduced by Piana et al (2007) rather elegantly addresses this issue by reversing the order of Fourier and spectral inversions. The (regularized) spectral inversion from count data to electron flux information is first performed at sampled points *in the spatial frequency domain*, i.e., on the count visibility spectra $V(u,v;\varepsilon)$, to produce a set of "electron flux visibilities" W(u,v;E) which, by construction, necessarily vary smoothly with E. Standard image-reconstruction packages can then be used to produce the desired electron flux image cube F(x,y;E) from the W(u,v;E). Since the F(x,y;E) have been constructed from visibilities that (unlike their photon counterparts) vary smoothly with energy, the resulting image cube will also vary smoothly

with E, thus facilitating the inference of information pertinent to the physical processes associated with the acceleration and transport of the electrons.

Petrosian & Chen (2010) applied this method to the 2003 November 3 solar flare (Fig. 2.1.1-1) to obtain the looptop and footpoint *energetic electron flux* spectra (Fig. 2.1.1-2 left). They argue that the electrons are accelerated (in their model through turbulence) at or near the looptop region, where they produce thin-target X-ray emission; the electrons then escape downward to the dense footpoint regions where they undergo Coulomb collisions and produce thick target X-ray emission. The results predict the presence of strong scattering and a high density of turbulence energy with a steep spectrum (Fig. 2.1.1-2 right) in the acceleration region for this mechanism to be operative.

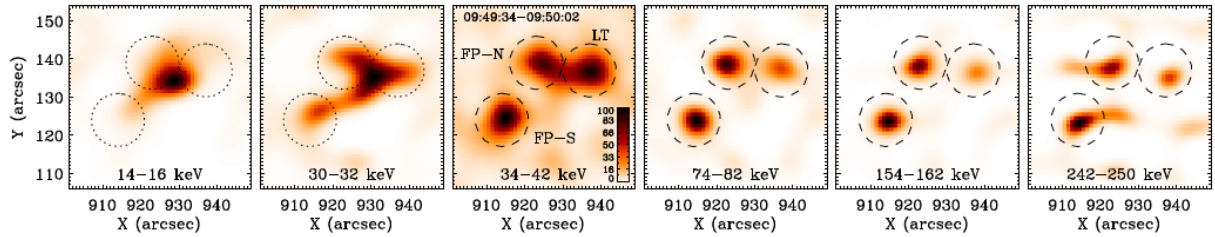

Figure 2.1.1-1. Electron flux spectral images (with 8 keV bin width above 34 keV and 2 keV bin width at lower energies) up to 250 keV in the 2003 November 03 flare during the nonthermal peak as reconstructed from two sets of the regularized electron visibilities by the MEM NJIT algorithm. The images show one LT and two FP sources above 34 keV and a loop structure at lower energies. Three circles are used to extract the LT and FP electron flux spectra above 34 keV (see Figure 2.1.1-2 left).

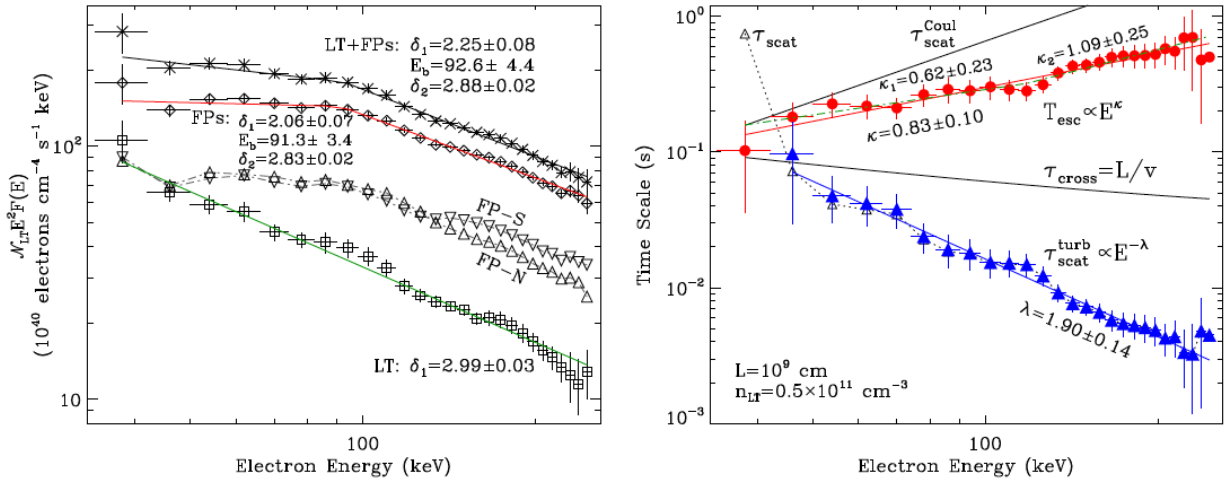

Figure 2.1.1-2. Left: Electron power spectra NLTE2F(E) for the loop top (LT) (square), the two footpoint (FPs) summed (diamond), and all three sources (LT + FPs, cross) in the 2003 November 03 flare. The LT spectrum can be fitted by a power-law, and the summed FP and total spectra by a broken power-law. Also note that the southern FP spectrum (downward triangular) is flatter than the northern FP spectrum (upward triangular), mostly above 90 keV by 0.3 in the power-law index, consistent with their asymmetric locations with respect to the LT. Right: Escape time (filled circle) and turbulence scattering time (filled triangular) in the (LT) acceleration region. The escape time can be well fitted by either a power-law or a broken power-law (dash dot) increasing with energy, and the turbulence scattering time by a power-law rapidly decreasing with energy. Also shown are the crossing, Coulomb scattering, and the mean scattering (open triangular) times. The reduced chi-squares for all the fittings are below or around 1.

Hurford, G. J., et al. 2002, Sol. Phys. 201, 61
Massone, A. M. et al. 2009, ApJ, 703, 2004.
Piana, M. et al. 2007, ApJ, 665, 846
Piana, M. et al. 2003, ApJ, 595, L127.
Schmahl et al. 2007, Sol. Phys., 240, 241
Xu, Y. et al. 2008, ApJ, 673, 576.
Petrosian, V. and Chen, S., 2010, ApJL, in press (arXiv:1002.2673).

2.1.1.2 Photospheric Compton Scattering of X-rays (Albedo)

Since the solar atmosphere above HXR sources is optically thin, the observed bremsstrahlung X-rays are often interpreted as directly related to the emitting electrons. However, the photons emitted downwards, toward the denser layers of the atmosphere, interact with free or bound electrons, and a fraction of them are scattered back toward the observer. This albedo component can account for up to 40% of the detected flux in the range between 30 and 50 keV, and thus must be taken into account when determining the photon spectrum from the primary source. It also affects the imaging since the albedo will be spread out over a larger area depending on the primary source's altitude.

Albedo: spectral properties

Kontar et al. (2006) have developed and implemented an albedo correction algorithm using a Green's function method for spatially integrated RHESSI X-ray spectra. This is now part of the standard RHESSI spectral analysis software, OSPEX, available in the Solar SoftWare (SSW). Sui et al. (2007) used this facility in a study of nine flares showing spectral flattening at low energies. They found that albedo from isotropically emitted photons could account for this flattening for three of the flares. Kontar et al. (2008) found 18 solar flare spectra that exhibit a statistically significant local minimum (a dip) in the range of 13-19 keV, a feature discovered thanks to the fine RHESSI energy resolution. The positions on the solar disc and the spectral indices of these events indicate that such features are likely to result from of photospheric albedo and not from a low-energy cutoff in the spectrum of the parent electrons as was originally thought. With the isotropic albedo correction applied, the low-energy cutoffs in the mean electron spectra for these flares must be less than ~12 keV.

The intensity of the albedo component compared to that of the primary X-ray source provides information on the directionality of the primary X-ray source, and hence on the degree of electron beaming. Application of this spectrometry method by Kontar and Brown (2006) showed that for two strong X-ray bursts observed by RHESSI the ratio of downward and upward propagating X-ray emitting electrons is close to one over a wide range of energies. This is in contrast to the standard thick-target model where significant electron beaming would be expected, certainly at the higher energies. This result and others prompted Brown et al. (2009) to suggest that the X-ray source electrons could be locally and continuously reaccelerated with near isotropy along the entire length of a magnetic loop. Such a model would also solve other difficulties of the thick-target model, such as the problematic high beam density and currents involved. The recent development in X-ray visibilities in combination with advanced Monte Carlo albedo simulations suggests that over the next few years albedo could become a dominant method to diagnose the electron pitch-angle distribution.

Albedo: spatial properties

Since the reflected X-rays come from a relatively large area, the surface brightness of the albedo patch at the solar surface is low compared to the directly detected primary compact source. This fact explains the difficulty in directly imaging the albedo patch (Schmahl & Hurford, 2002), but highlights the importance of the inclusion of albedo for understanding the measurements of the source positions and sizes (first and second moments), and the quantities integrated over the area. Kontar and Jeffrey (2010) have developed a Monte-Carlo code to simulate the spatial properties of an X-ray source in the presence of albedo. The results show that for X-ray sources at 1 Mm above the photosphere, the source positions are shifted by 0.1-0.4" radially toward the disk center and the sources are enlarged by up to ~250% even for an isotropic source where the albedo effects are lower than for more downward directed emission. As an example, for a disk-centered point source at a height of 1.0 Mm (1.4") above the photosphere, the FWHM extent of the measured source size will be as large as 6.9" in the 20-50 keV range. The source size and position changes are the largest for flatter primary X-ray spectra, stronger downward anisotropy, sources closer to disk center, and for energies between 30 and 50 keV. Albedo must be taken into account when X-ray footpoint positions, footpoint motions, or source sizes are determined from X-ray images, and provides a natural explanation for flare footpoint sources being more extended in X-rays than in optical or EUV ranges.

The detection of 20 – 100 keV X-ray footpoint sources extended by <4" reported by Dennis and Pernak (2009) is, therefore, surprising and may indicate that the sources are at lower altitudes than predicted by the thick-target model.

Brown, J. C. et al. 2009, A&A, 508, 993-1000.
Dennis and Pernak, 2009, ApJ, 698, 2131-2143.
Kontar et al. 2006, A&A., 446, 1157-1163.
Kontar et al. 2008, Sol. Phys., 252, 139-147.
Kontar and Jeffrey, 2010, A&A, submitted, arXiv:1003.0884.
Schmahl, E. and Hurford, G. J., 2010, RHESSI Science Nugget 119
Sui, L., Holman, G. D., & Dennis, B. R. 2007, ApJ, 670, 862

2.1.1.3 Spectral Analysis

Soft-hard-harder (SHH) spectral evolution and SEP events observed near 1 AU

Kiplinger (1995) found that flares with HXR burst spectra that evolved in time from soft to hard to harder (SHH) are closely associated with high-energy SEP events observed in interplanetary space, with a 96% success rate in predicting large proton events. If the SHH pattern was seen in a HXR burst, a proton event was almost sure to happen, strongly suggesting a physical connection between the X-ray-producing electrons in the flare (on the closed flare loops that create the magnetic mirror geometry) and the escaping energetic protons on open field lines. This correlation is puzzling, especially since it is generally believed that fast CME driven shock front, remote from the flare itself, is the main proton accelerator. In a statistical study of all RHESSI flares, Grayson et al. (2009) reach the same conclusion as Kiplinger (1995). They found that all RHESSI flares associated with an SEP event show SHH behavior, and none of the flares with SHS (normal) behavior are associated with an SEP event.

RHESSI images show that 20 to 100 keV X-rays originate from footpoints during times with SHH behavior (Saldanha et al, 2008, Grigis & Benz,. 2008). Thus, if coronal trapping is responsible for the gradual hardening, the hard X-ray emission is not produced by electrons in the corona but by electrons leaving the trap and precipitating to the footpoints. The position of the footpoints, sampling the motion of the acceleration region (Fig. 2.1.1.3-1), shows no abrupt behavior at the onset of the hardening (Grigis & Benz, 2008). Therefore, the same acceleration process taking place in the preceding impulsive phase appears to continue into the hardening phase. This brings into question previous scenarios suggesting a second acceleration process, possibly associated with the CME shock, at least as applied to the acceleration of electrons.

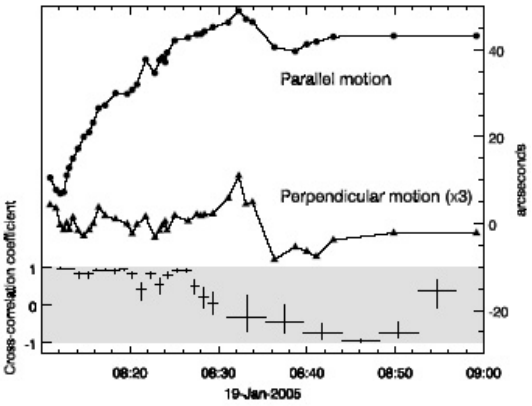

Figure 2.1.1.3-1 The motion of a flare X-ray footpoint is continuous during the sudden onset of the hardening phase at 08:29 UT, when the relation between spectral index γ and flux F changed from +1 (soft-hard-soft) to negative (soft-hard-harder) (Grigis & Benz 2008).

Grigis & Benz (2008) applied a transit-time acceleration model to interpret the hardening as a property of the accelerator. As the most likely parameter changing in the late flare phase, the electron energy has been identified, below which electrons are trapped in the accelerator. If this trapping energy increases, the electron flux precipitating to the footpoints and the photon spectral index decrease in agreement with observations. Therefore, the trapping time in the corona must be shorter than the collisional loss time, at least at energies below ~100 keV. Efficient trapping is observed at higher energies (>200 keV), and coronal emission can even dominate the footpoint emission during the decay phase of the HXR burst.

Grayson et al., 2009, ApJ, 707, 1588
Grigis & Benz, 2008, ApJ, 683, 1180
Kiplinger, 1995, ApJ, 453, 973
Saldanha et al. 2008, ApJ, 673, 1169

Non-uniform plasma ionization

Su et al. (2009) studied the downward break frequently observed in flare hard X-ray spectra between 20 and >100 keV. One possible explanation of this break is non-uniform plasma ionization in the thick-target emission region. They derived an upper limit on the magnitude of the spectral break that can be caused by such non-uniform ionization, and studied the shape of spectra at the time of the impulsive peaks of 20 flares. Fifteen of the twenty spectra showed a downward break with nine being consistent with non-uniform ionization. Six of the fifteen spectral breaks were found to have less than a 2.5% probability of being caused by non-uniform ionization alone and some other explanation such as a low energy cutoff in the parent electron spectrum must be invoked.

Su, Y. et al. 2009, ApJ. 705,1584

Superhot (T>30 MK) thermal flare plasmas

RHESSI's high spectral resolution (<~1 keV FWHM) allows the very steep spectra of hot thermal sources to be resolved, and enables the determination of the fluxes in the Fe and Fe/Ni line complexes at ~6.7 and ~8 keV. Caspi & Lin (2010) studied the thermal line and continuum emission in the 23 July 2003 X4.8 flare, and found two distinct nearly isothermal components - a super-hot component that reaches a peak temperature of ~44 MK early in the impulsive phase, and a cool (T~20 MK) component that tracks the GOES-derived temperature and emission measure within ~5% and ~20% throughout most of the flare. RHESSI imaging shows that these two thermal sources

are spatially separated, with the superhot generally elongated away and further away (and thus likely higher in altitude) from the footpoints than the cool component.

Caspi & Lin (2010), ApJL, in preparation.

2.1.1.4 HXR Source Motions: Evaporation, Oscillation, and Implosion

The RHESSI hard X-ray observations are able to precisely track source motions and thus probe the global structure of the flare, as related to the energy source and magnetic restructuring/reconnection. Early results showed that RHESSI could detect blobs of hot plasma rising and falling apparently along flux tubes, with important inferences about the evolution of chromospheric evaporation in the loop (Sui et al. 2006, Liu et al. 2006). In the 23 July 2003 X4.8 flare the dominant coronal non-thermal HXR source (with little or no footpoint emission) in the pre-impulsive phase showed downward motion that then reversed at the onset of the impulsive phase (Lin et al. 2003). Veronig et al, (2006) found that the looptop source in the 2003 November 3 X3.9 flare showed apparent downward motion early in the flare, that was consistent with a collapsing magnetic trap embedded in a 2D magnetic reconnection model. Studies of footpoint motions (e.g. Ji et al. 2008), making use of the HXR-emitting electrons as tracers of the evolution of the flaring magnetic structure in the impulsive phase, show decreasing footpoint separation initially, followed by the usual increasing footpoint separation later (Figure 2.1.1.4-1) - consistent with the concept of flare implosion as a source of magnetic energy release (Hudson, 2000).

More recently quasi-oscillatory HXR source motions have been reported by Zimovets and Struminsky (2009) for the X1 flare on 2005 Jan. 19. They show that the hard X-ray footpoints move along the flare ribbons during the oscillatory phase with each peak arising from a different location along the flare ribbons. This has been interpreted in terms of two different MHD models by Ofman & Sui (2006) and Nakariakov et al. (2006). Warmuth et al. (2009) also studied this same event and found that electron acceleration in the last major hard X-ray peak is different from that in the preceding peaks. There is no Neupert effect associated with this final peak, unlike for the previous peaks, and spectral fits indicate that the accelerated electrons have a low-energy cutoff above 100 keV. This peak is associated with the motion of one of the X-ray footpoints into a region of higher photospheric magnetic field strength and shows SHH spectral evolution. It is also associated with the onset of 200 – 800 MHz continuum radio emission. The model of Nakariakov et al. has subsequently been applied to other flares showing quasi-periodic oscillations in the RHESSI hard X-ray flux (Inglis & Nakariakov 2009; Nakariakov and Melnikov 2009).

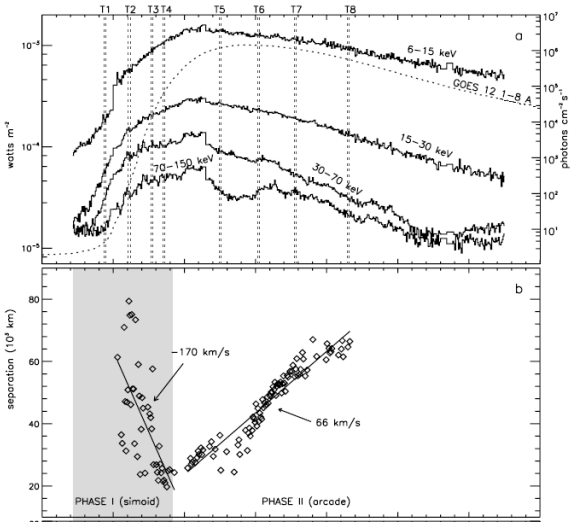

Fig. 2.1.1.4-1. Time profiles and source heights for the X10 flare of 2003 October 29 (Ji et al. 2008). The early phase clearly shows downward motions consistent with the implosion likely to be associated with magnetic reconnection.

Hudson, 2000, ApJ 531, L75
Inglis, A. R., & Nakariakov, V. M. 2009, A&A, 493, 259
Ji, H. et al. 2008, ApJ 680, 734
Lin, R.P. et al. 2003, ApJ, 595, L69
Liu, W. et al. 2006, ApJ, 649, 1124
Nakariakov, V.M. et al. 2006, A&A 452, 343
Nakariakov, V.M., & Melnikov, V. F. 2009, Space Sci. Rev., 149, 119
Ofman, L. and Sui, L. 2006, ApJ, 644, L149
Sui, L. et al. 2006, ApJ, 645, L157
Warmuth, A. et al. 2009, Ap. J. 699, 917
Zimovets, I. V. and Struminsky, A. B. 2009, Solar Phys. 258, 69

2.1.1.5 Electron Acceleration during Magnetic Reconnection

HXR observations show that the accelerated tens-of-keV electrons often contain >~10-50% of the total energy released in the flare, implying that electron acceleration is intimately related to the energy release process (Lin & Hudson, 1976), presumably magnetic reconnection occurring in the corona above the flare loops. In the last few years, very significant progress has been made in the understanding of collisionless magnetic reconnection, through in situ space measurements, laboratory studies, and extensive theory and simulation work. Recently, the long-standing problem - to explain how energetic electrons are efficiently produced as magnetic fields reconnect and release energy - has been addressed by Drake et al (2006a). Particle-in-cell simulations of reconnection show that

the narrow current layers form at the X-line and produce secondary magnetic islands (Drake et al 2006b) that result in strong electron energization. While some acceleration comes from parallel electric fields, the primary energy gain is due to the contraction of the initially squashed magnetic islands. Electrons circulating rapidly within the islands gain energy through a Fermi process, by reflecting off the ends of the islands as they move inward at the Alfvén speed. Up to 60% of the released magnetic energy is transferred to the electrons in the process. These islands must fill a large volume to accelerate the number of electrons required for a flare.

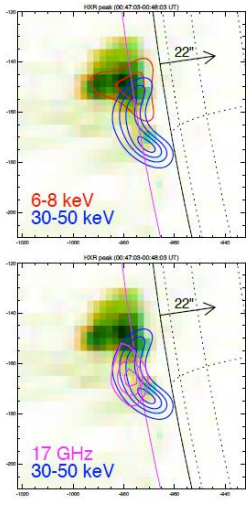

Figure 2.1.1.5-1. X-ray and microwave imaging during the hard X-ray peak (00:47:50-00:48:10 UT). Top: RHESSI contours in the thermal (6-8 keV, red) and the non-thermal (30-50 keV, blue) range are shown on an EIT 195A image taken just at end of the main hard X-peak (00:48:11 UT) with the pre-flare emission subtracted. Bottom: Microwave contours (magenta) at 17 GHz are shown on the same EIT image. For comparison, the 30-50 keV source seen during the impulsive phase is shown as well (blue). The magenta curve gives the location of the limb at 17 GHz. The black arrows indicate the occultation height.

Recently RHESSI detected an intense coronal HXR source located about 6 Mm above the flare loops in the 2007 December 31 flare (Fig. 2.1.1.5-1), where the footpoints were occulted but with STEREO providing un-occulted EUV imaging of the whole flare (Krucker et al.. 2010). This HXR source had a non-thermal power-law spectrum with no detectable thermal emission, and it filled a volume of ~10^{27} cm^3 with a non-thermal, >16 keV electron density of ~$2x10^9$ cm^{-3} for a total of ~$2x10^{36}$ electrons. Microwave observations from Nobeyama show a co-spatial source (Fig. 2.1.1.5-1, bottom), consistent with gyrosynchrotron emission from the high-energy tail of the same power-law electron distribution. The magnetic field in the source, estimated from the turnover in the radio spectrum, is ~30-50 Gauss, implying that the energy density of the non-thermal electrons in the source is comparable to that of the magnetic field, as predicted by Drake et al's model. Thus, this above-the-looptop source is likely to be the coronal acceleration region for the flare. Other similar above-the-looptop coronal HXR sources (such as in the Masuda flare) have been detected, but RHESSI's high spectral resolution is required to show that the source is non-thermal.

Drake, J.F. et al. 2006a, Nature, 443, 553.
Drake, J.F. et al. 2006b, Geophys. Res. Lett. 33, L13105
Krucker et al. 2010, ApJ, submitted.
Lin, R. P. and Hudson, H. S., 1976, Solar Phys., 50, 153

2.1.1.6 Coronal Hard X-ray Emission

Partially Disk-occulted Flares

A survey of RHESSI observations (Krucker & Lin 2008) of 55 partially disk-occulted flares reveal that 90% show two components in the HXR range - thermal emission at lower energies and additional emission extending to higher energies with fast time variations and a soft spectrum. Krucker & Lin (2008) suggest that, at least in some events, the rapidly-varying component could be produced in the thin-target scenario (i.e. faint HXR production without significant collisional energy losses) by the same population of electrons that later precipitate and lose their energy by collisions in loop footpoints (thick target).

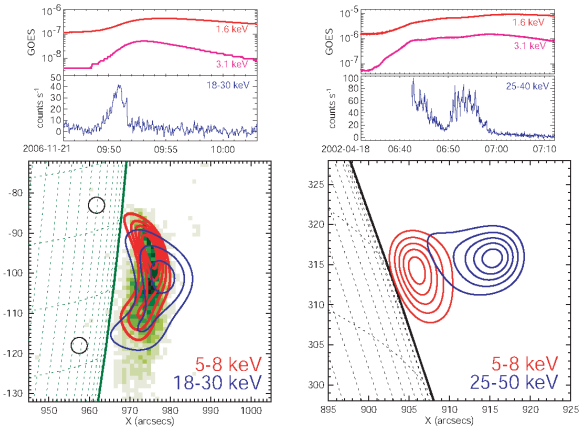

Fig. 2.1.1.6-1. Two examples of RHESSI X-ray observations of partially occulted flares. Top panels: GOES soft X-ray (red) and RHESSI hard X-ray (blue) time profiles. Bottom panels: RHESSI imaging results with thermal emission in red and nonthermal emission in blue.

A typical example is shown in the left panels of Fig. 2.1.1.6-1, where thermal emission originates from a simple loop at the western limb. Above 18 keV, faint nonthermal

emission with fast time variations (of the order of tens of seconds) is seen that comes from a loop ~2,000 km above the thermal loop observed at the same time. However, the nonthermal loop agrees well in altitude with the thermal flare loop seen later, at the time of the soft X-ray peak. This is consistent with simple flare models (from Krucker et al. 2007).

The right panels of Fig. 2.1.1.6-1 show a rare example where the nonthermal emission originates clearly from above the thermal flare loops (~8,000 km above in this case), similar to the Masuda flare (Masuda et al. 1994). However, later in this event, the thermal loops never reach the altitude of the nonthermal source. This behavior is clearly different from the standard flare model, and is currently not understood.

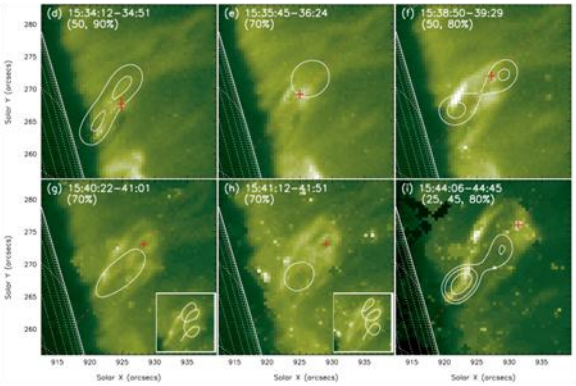

Figure 2.1.1.6-2. Episodic splitting of the coronal X-ray source in the partially occulted 2003 Apr. 24 flare with an associated prominence eruption (from Liu et al. 2009). RHESSI 3 – 6 keV contours are superimposed on TRACE 195 Å images for four different times. The red crosses mark the location of the filament apex. The boxes in frames (g) and (h) show a zoomed-in tracing of the helical structure of the prominence.

Another example of a partially occulted flare observed by RHESSI on 2003 April 24 is shown in Figure 2.1.1.6-2. This flare was associated with a prominence eruption, and has been studied by Liu et al. (2009). The initially single coronal source split into a double source several times during the evolution of the flare when the energy release rate was greatest. When the source was split, the lower source had a lower temperature and harder nonthermal X-ray spectrum than the higher source. The two sources showed an energy dispersion similar to that observed by Sui & Holman (2003) until the energy at which the X-ray emission became nonthermal was reached. The energy dispersion reversed above that energy. This indicates that the nonthermal X-ray emission did not arise predominantly from the reconnection region presumably located between the two X-ray sources.

Krucker, S. et al. 2007, ApJL, 671, 193
Krucker, S. & Lin, R. P., 2008, ApJ, 673, 1181.
Liu, W. et al., 2009, ApJ, 698, 632-640.
Masuda et al., 1994, Nature, 371, 495.
Sui, L., & Holman, G. D. 2003, ApJ, 596, L251

2.1.2 White-light Flares

The visible continuum emission of a flare (the "white light flare") and its extension into the near UV contain most of a flare's radiative energy (e.g. Emslie et al. 2005; Hudson et al. 2010). RHESSI data confirm that the impulsive-phase acceleration of electrons coincides well in space, time, and energy content with the white-light flare (Fletcher et al., 2008; Krucker et al 2009) Watanabe et al.(2010) compared the radiative losses in white-light with the energy deposition rate in flare-accelerated electrons for four different time interval during the December 13, 2006 flare (Fig. 2.1.2-1) and found a linear correlation suggesting a close connection between the HXR and white light emission. For cut-off energies below 40 keV, the energy in flare-accelerated electrons is large enough to account for the radiative losses.

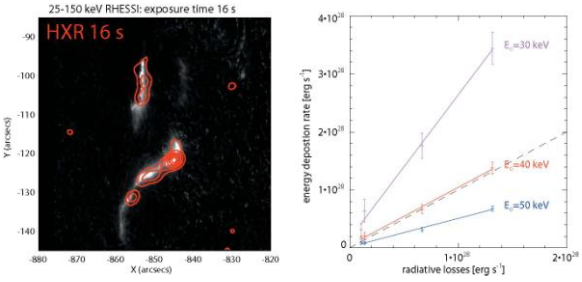

Figure 2.1.2-1. Left: HINODE/SOT G-band observations of the December 6, 2006 white-light flare is shown as an image with RHESSI HXR contours (25-150 keV) over plotted in red. The two emissions show the same sources along the flare ribbons. **Right**: comparing the radiative losses in white-light with the energy deposition rate in flare-accelerated electrons for four different time interval during the December 13, 2006 flare (Watanabe et al. 2010). The different colors represent values derived from the indicated cut-off energies (E_o) in the electron spectrum.

Xu et al. (2006) reported unexpectedly strong near-infrared continuum at 1.56μm (corresponding to the deepest photosphere in the undisturbed atmosphere). It appears that the white-light continuum in the impulsive phase basically is Paschen continuum from hydrogen recombination, in which the bulk of the energy is in the near-UV Balmer continuum with a characteristic temperature of order 10^4 K (Hudson et al. 2010). This suggests that "back-warming" from this optical continuum amounts to a change in the temperature of the photosphere (Lindsey & Donea 2008), with dynamic consequences that possibly include the seismic waves

discussed below. Isobe et al. (2007) have noted the likelihood of 3D structures with unknown theoretical implications. The observations have led to new theoretical developments, with coupling between particle hydro codes (Liu et al. 2009), high time resolution (Kasparova et al. 2009), and consideration of the effects of evaporation (Milligan and Dennis 2009; Liu et al. 2010).

Emslie, A.G. et al. 2005, JGR 110, A11103
Fletcher, L. & Hudson, H.S. 2008, ApJ 675, 1645
Hudson, H.S. et al. 2010, ArXiv 1001.1005
Krucker et al. 2009, SPD mtg. 40, #19.19
Watanabe et al. 2010, ApJ, in preparation

2.1.3 Explosive Chromospheric Evaporation

Combining observations from RHESSI and the EUV Imaging Spectrometer (EIS) on Hinode has allowed a comprehensive diagnosis of the chromospheric response to a flare to be made. For the impulsive phase of a C1.1 flare on 2007 December 14 Milligan & Dennis (2009) used EIS data to determine the evaporation velocity for a number of emission lines formed over a broad range of temperatures at the site of the HXR footpoints (see Figure 2.1.3-1). They found red shifts (corresponding to downflows) for lines formed at temperatures below 1.8 MK and blue shifts (upflows) for lines formed at higher temperatures. The measured plasma flows were deemed to be due to sustained energy deposition from nonthermal electrons. By fitting a thick-target power-law electron spectrum to the RHESSI count-rate spectra, the incident electron flux was estimated to be $>5 \times 10^{10}$ erg cm^{-2} s^{-1}, in agreement with the flux required to drive explosive chromospheric evaporation according to hydrodynamic simulations.

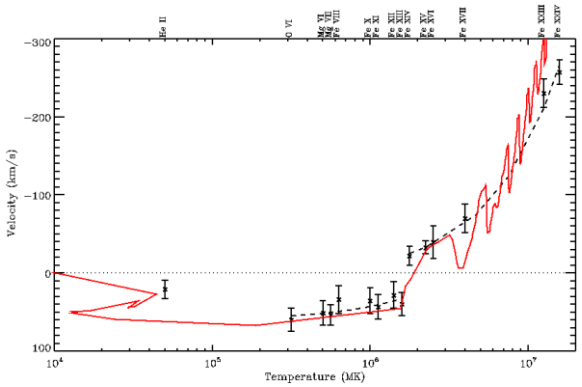

Figure 2.1.3-1. Temperature dependence of plasma velocities determined from the line shifts seen in the EUV lines indicated as measured with Hinode/EIS. Broken lines are linear fits to the separate upflow and downflow velocities vs. temperature. Red line shows predictions of a model by Liu et al. (2009).

The transition temperature between downflowing and upflowing plasma is significantly higher than previously found but is in agreement with the predictions of the Liu et al. (2009) model of the chromospheric response to explosive evaporation that incorporates electron deposition. It shows that the underlying chromosphere is also heated to temperatures approaching 2 MK, in agreement with the observations. Thus, the temperature at which the sign of the Doppler velocity changes may not necessarily be an indicator of the depth at which the bulk of the electron energy is deposited, as was previously thought, but rather depends on the duration and/or magnitude of the energy deposition at the footpoints.

Brown et al. 2009, A&A 508, 993
Fletcher, L. & Hudson, H.S. 2008, ApJ 675, 1645
Hudson, H.S. et al. 2010, ArXiv 1001.1005
Isobe, H. et al. 2007, PASJ 59, S807
Kasparova, J. et al. 2009, A&A 499, 923
Lindsey, C. & Donea, A. 2008, Sol. Phys. 251, 627
Liu, W. et al. (2009), ApJ, 702, 1553
Liu, S. et al. (2010), ApJ, 709, 58
Milligan, R. O. and Dennis, B.R. 2009, ApJ 699, 968
Xu, Y. et al. 2006, ApJ, 641, 1210.

2.1.4 Excitation of seismic waves

Solar flares are believed to be the source of local seismic events on the solar surface called “sunquakes” that were first detected using SOHO-MDI (Kosovichev & Zharkova 1995, 1998). Although the total energy in these acoustic waves probably does not exceed 10^{-3} of the total flare energy, it is unknown how even this much gets coupled from the tenuous corona into the ponderous photosphere. Observationally, the data are quite consistent with an impulsive-phase origin – a close association with white-light flaring and RHESSI hard X-rays has been established (see Figure 2.1.4-1), and thus by inference the acceleration of fast CMEs (e.g. Temmer et al. 2010). Multiple mechanisms have been proposed to explain these phenomena, varying from chromospheric shocks generated by electron beams, heating of the photosphere by protons and/or electrons, to dynamical changes of the magnetic fields (Hudson et al., 2008). Donea and Lindsey (2005) and Moradi et al. (2007) found that all seismic events have a white-light component, but not all white-light events are seismically active. Using RHESSI

observations of two flares, Martinez-Oliveros et al. (2007, 2008) found that the origin of the seismic activity is co-spatial with hard X-ray footpoints suggesting that the HXR-producing electrons are likely playing an important role in the generation of sunquakes. A statistical study comparing seismic activity and HXR/γ-ray emission observed by RHESSI of all large RHESSI flares is currently in preparation.

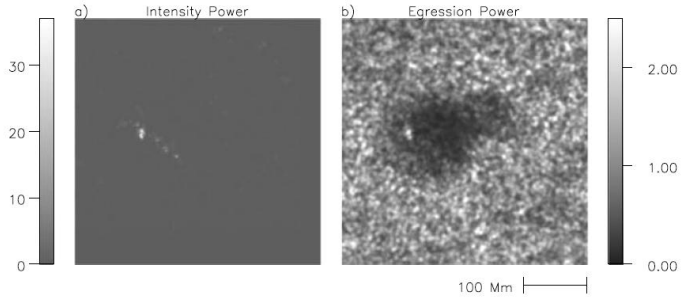

Figure 2.145-1. White-light flare image (left), Fourier-filtered to match the 5-7 mHz bandpass of the seismic observations (right), showing excellent agreement for the flare acoustic source located in the sunspot umbra (Donea and Lindsey, 2008). These sources agree well with the RHESSI hard X-ray positions and timing.

Donea, A.-C. and Lindsey, C., 2005, ApJ, 630, 1168.
Hudson et al. 2008, ASP Conf. Proc. 383, 221.
Kosovichev, A. and Zharkova, V., 1995, Helioseismology. ESA SP, 376, 341.
Kosovichev, A., and Zharkova, V.,1998, Nature, 393, 317.
Martinez-Oliveros, J. et al. 2007, Solar Physics, 245, 121.
Martinez-Oliveros, J. et al. 2008, Solar Physics, 251, 613.
Moradi, H. et al. 2007, MNRAS, 374:1155.
Temmer, M. et al. 2010, in press (ArXiv 1002.3080v1)

2.1.5 Gamma-Ray Imaging and Spectroscopy

In 2009, a new round of Monte Carlo simulations was undertaken to produce a new model of RHESSI's instrument response to higher-energy photons and correct an error. These simulations, which required nearly a year of CPU time, were accomplished in a few weeks with the use of a Beowulf computing cluster that was taken over from another project by the RHESSI team for this task. The range of the simulations was extended from the original limit of 20 MeV to 150 MeV to accommodate modeling the response of the instrument to pion-produced gamma rays, and enable the study of flare emissions up to energies of a few hundred MeV, important for the extremely energetic flares such as 20 January 2005. The spectroscopic analysis has also been significantly improved using the new gamma-ray line production code of Murphy et al. (2009).

Murphy, R. J. et al. 2009, ApJS, 183, 142.

2.1.5.1 Flare on 2003 October 28

Chromospheric Abundances and Accelerated Particle Composition

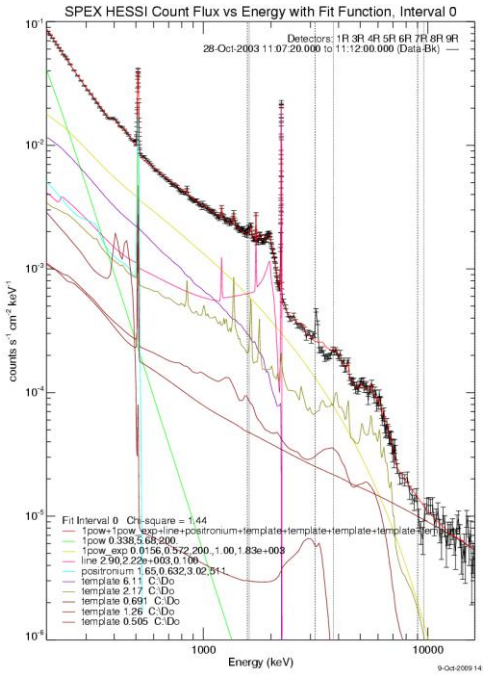

Fig. 2.1.5-1 Fit to the 2003 October 28 gamma-ray spectrum showing the best fitting components.

The gamma-ray spectrum of the 2003 October 28 flare (Figure 2.1.5-1) has been fitted above 200 keV with several different components: bremsstrahlung represented by the sum of a single power law and a power law with an exponential cutoff; 0.5, 2.2 MeV, and alpha - ^{4}He lines; a solar Compton-scattered 2.2 MeV continuum; gamma-ray emission templates for proton and alpha-particle interactions on assumed ambient compositions (e.g. Asplund photospheric or coronal); and templates for heavy accelerated particles interacting with ambient H and He. These nuclear-emission templates were calculated for the heliocentric angle of the flare and for various values of α/p and proton spectral index. The spectrum is best fit for an ambient abundance that is similar to that found in gradual SEP events (e.g. coronal composition) and for an accelerated particle composition that also is similar to that found in gradual SEP events. This suggests that FIP fractionation in this flare occurred deep in the chromosphere and that the source of accelerated particles that interacted were drawn from the corona.

The accelerated particle spectral index and α/p ratio were obtained by fitting several-hundred emission templates to the data. The χ^2 contours indicate that the best-fit power-law index is 3.8±0.5 and α/p ratio is 0.30 ± 0.15. The latter ratio appears to be significantly higher than that observed in most SEP events.

2.1.5.2 Flare on 2005 January 20

Distinct Phases of Particle Acceleration and Long-Term Particle interaction at the Sun

The 2005 January 20 flare was accompanied by a Ground Level Event (GLE) where protons with energies in excess of 5 GeV were observed at Earth within 6 minutes of the onset of the impulsive phase of the flare. RHESSI's spectroscopic measurements have revealed two distinct phases of particle acceleration during the few minutes of the flare. Bremsstrahlung HXRs from what appears to be the closed-loop phase of the flare was first observed just before 06:44 UT and peaked just before 06:46 UT. In Figure 2.1.5-2 the nuclear de-excitation time profile before 06:45:40 UT was fit with a loop model using the bremsstrahlung HXR profile as a proxy for the ion acceleration profile. The red curve shows the calculated nuclear flux for the fitted time interval and extension to later times. A second particle-acceleration phase commencing at ~06:45:40 UT is suggested by the striking increase in >20 MeV photons observed by both RHESSI and Coronas (Masson et al. 2009). We then assumed that the profile of >20 MeV gamma-rays from Coronas (blue curve) reflected the particle acceleration history of the second acceleration phase, and normalized it so that the total of the two calculated fluxes (green) curve agreed with the observed nuclear de-excitation fluxes.

We performed a similar analysis but this time compared calculated time profiles for the two components with the observed fluxes in the neutron capture line, taking into account the delay in the capture line due to the ~100 sec slowing down time of the neutrons. The results (Figure 2.1.5-2 bottom) show that the second acceleration phase dominates the generation of the neutron capture line, indicating a significantly harder particle spectrum. The inferred spectral index of the protons was ~3.9 in the closed-loop component, and 3.1 in the second acceleration phase, and ~10^{32} protons >30 MeV were accelerated in the closed-loop phase while ~6×10^{32} protons >30 MeV were accelerated in the second phase up until 06:52 UT. For comparison, Mewaldt (private comm.. 2007) estimated that there were ~2×10^{34} protons >30 MeV in the entire SEP event.

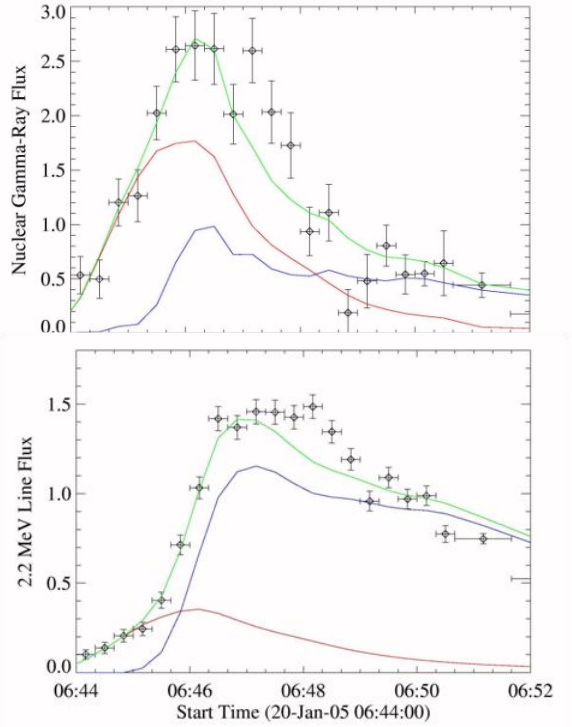

Fig. 2.1.5-2. Top: time profile of the total nuclear de-excitation gamma-ray flux (cm^{-2} s^{-1}). The curves show the calculated contributions from the first particle acceleration phase (red), second phase (blue) and total (green). Bottom: Time profile of the 2.2 MeV neutron-capture line flux (cm^{-2} s^{-1}). The curves have the same color code as for the top plot.

The rise time of the second acceleration phase appears similar to that observed in the neutron monitor rates observed at the South Pole (Tylka, private comm.), suggesting this second phase is associated with the injection of high-energy particles into space. RHESSI has imaged both hard X-rays and the neutron-capture line (Hurford et al 2006) between 06:44 and 06:56 UT (Figure **2.1.5-3),**

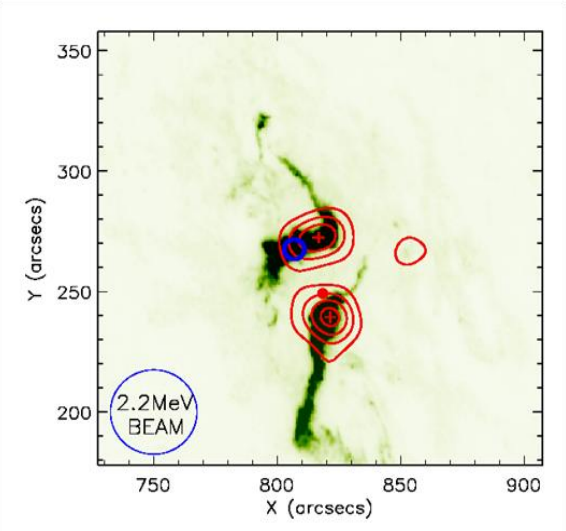

Fig. 2.1.5-3. RHESSI image of the 2005 January 20 flare. Red contours: HXR sources, blue circle, centroid of 2.2 MeV source.

showing that the hard X-rays primarily come from two foot points, but the 2.2 MeV line photons appear to come from a region centered near the northern foot point. If the protons had been accelerated in closed loops, the 2.2-MeV centroid should lie between the two footpoints. Since most of the 2.2 MeV line photons were produced during the second acceleration phase and almost all of the RHESSI observed 2.2 MeV line photons were imaged so there is no missing extended source of emission, it is interesting to speculate that the protons in this second phase came from the same acceleration process that produced protons in the GLE - only a fraction of them were able to reach the solar surface via open field lines that happened to be close to the northern foot point.

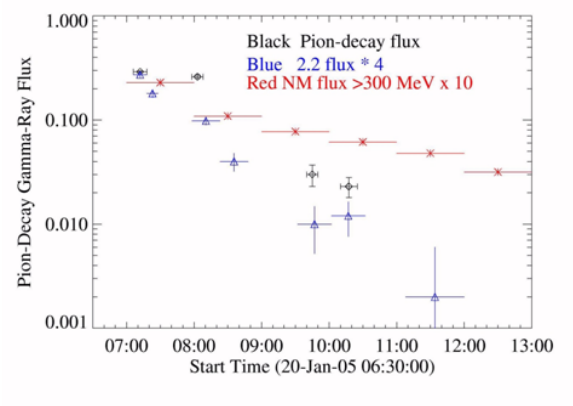

Figure 2.1.5-4. Long-duration gamma-ray emission from the 2005 January 20 flare observed in both the 2.2 MeV line and continuum attributed to pion-decay emission by RHESSI. For comparison we also show the GOES HEPAD >300 MeV time history.

After 06:52 UT the spectrum of interacting particles hardened significantly, so that by ~07:05 UT the power-law spectral index reached ~2.5. There is evidence that at later times the index may harden further, close to the event-averaged SEP index of 2.15. Gamma-ray emission from this event has been observed by RHESSI up until at least 10:30 UT (Figure 2.1.5-4), over 3.5 hours after the onset of the flare both in the 2.2 MeV capture line and in what appears to be pion-decay emission observed in the RHESSI spectroscopic energy range. Also shown is the proton flux >300 MeV observed by neutron monitors (Tylka, private comm.). The number of interacting protons >30 MeV interacting at the Sun after 07:00 UT is comparable to the number that interacted at the Sun before that time.

Masson, S., et al. 2009, ApJ, 700, 559

2.1.5.3 Correlated >0.3 MeV Electron and >30 MeV Ion Acceleration

Shih et al. (2009) analyzed all RHESSI measurements from 2002 to 2005 (29 flare events) of the 2.223 MeV neutron-capture gamma-ray line and >0.3 MeV electron bremsstrahlung continuum emissions, produced by >30 MeV accelerated protons (depending on assumptions) and >0.3 MeV accelerated electrons, respectively. The two emissions were found to be closely proportional over >3 orders of magnitude in fluence, from the largest flares down to the limits of detectability (Figure 2.1.5-5); all flares fall (<1σ) within a factor of two of the best-fit line, except for four flares with marginal (~1–2σ) line detections.

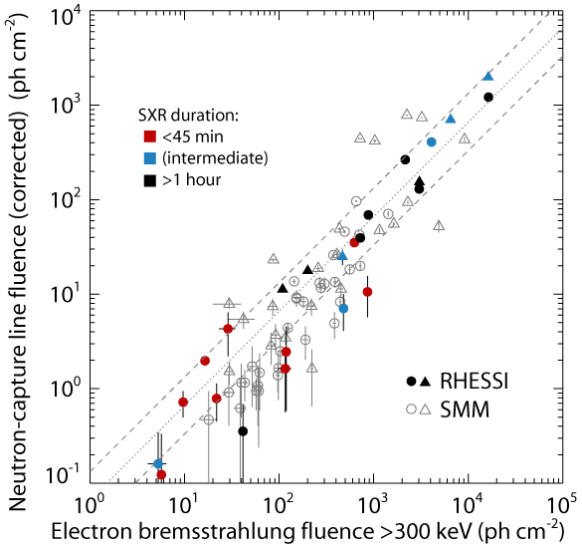

Figure 2.1.5-5 Correlation plot between neutron-capture line fluence (corrected for limb darkening) and >300 keV bremsstrahlung fluence for flares with heliocentric angles <80°. Circles (triangles) represent flares with complete (incomplete) coverage. The dotted line indicates the best-fit line in linear space that passes through the origin, with a ratio of 0.066, and the dashed lines differ by a factor of 2 in intensity from the best-fit line.

There is also a close proportionality between the 2.223 MeV fluence and the peak GOES 1–8 Å soft X-ray (SXR) flux, but only above a 2.223 MeV threshold fluence of 50 photons cm^{-2} (equivalent to ~2×10^{31} protons >30 MeV). Below this threshold, the flares usually have large (M-class or higher) but generally uncorrelated excess SXR emission.

Thus it appears that the acceleration of >30 MeV protons is always closely proportional to the acceleration of relativistic (>0.3 MeV) electrons, while the acceleration of non-relativistic electrons (that presumably heat the plasma that emits the SXRs) is only proportional when the proton acceleration exceeds a threshold. Shih et al (2009) notes that all flares that accelerate enough >30 MeV protons to be detected by RHESSI are accompanied by ~M-class or X-class SXR emission. Smaller C-class and lower flares that are "scaled down" versions of the large gamma-ray line flares but without excess >50 keV and SXR thermal emission, are lacking.

The observations thus are consistent with two (possibly concurrent) acceleration processes: one that always accelerates both >30 MeV protons and >0.3 MeV electrons

proportionally, and a second that accelerates electrons above 50 keV but not above 300 keV. In larger, M- or X-class flares, when more than ~2×10^{31} protons are accelerated above 30 MeV, the fraction of energy going to low-energy acceleration and thermal plasma reaches a constant minimum.

The electron-to-proton ratios – J_e(0.5 MeV)/J_p(10 MeV) – in these flares, obtained from the gamma-ray observations, are about two orders of magnitude larger than the ratios in gradual SEP events, but are comparable with ratios in impulsive SEP events. This difference is consistent with the paradigm where impulsive SEPs are linked to flare acceleration, while gradual SEPs are accelerated through a different mechanism. However, impulsive SEP events have rarely, if ever, been detected from a gamma-ray line flare, and RHESSI has not detected any gamma rays from the flares associated with the impulsive events.

Shih, A. Y. et al., 2008, ApJ, 698, L152.

2.1.5.4 Gamma-ray and radio sub-millimeter observations

Observations of the sub-millimeter emissions of solar flares above 200 GHz (Kaufmann et al. 2004, Luethi et al. 2004) have revealed a second component with intensities well above an extrapolation of the synchrotron spectrum seen at lower frequencies. Surprisingly, the measurements at two frequencies suggest that the spectrum of this new component increases with increasing frequency in contrast to the synchrotron spectrum. This exciting new finding has prompted many theoretical explanations (e.g. Fleishman & Kontar 2010) but the emission mechanism of this new component is currently unclear.

Several studies have been published investigating the relationship of this new sub-mm component with HXR and γ-ray emissions seen with RHESSI (Silva et al. 2007, Trottet et al. 2008, Kaufmann et al. 2009, Giménez de Castro et al. 2009). The onset of the impulsive component of the radio sub-millimeter emission during the giant flare of October 28, 2003 is simultaneous with the start of high-energy (>200 MeV/nucleon) proton acceleration and the production of pions. The 210 GHz source size is compact (<10 arcsec) and its location is co-spatial with the 2.2 MeV footpoint emission seen by RHESSI (fig. 2.1.5-6). The close correlation in time and space of the submm emission with the production of pions suggests that synchrotron emission of positrons produced in charged-pion decay might be responsible for the observed compact radio source. However, order-of-magnitude approximations suggest that the derived number of positrons from charged-pion decay is probably too small.

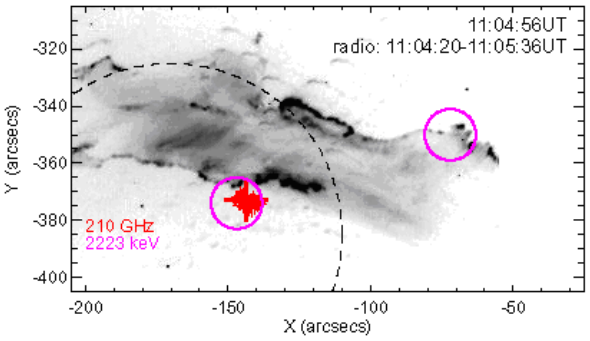

Figure 2.1.5-6. Imaging in radio, UV, and gamma-rays during the October 28, 2003 flare (from Trottet et al. 2008). The TRACE 1600Å image is shown with 210 GHz centroid positions over-plotted as red crosses. The average position and source size of the radio emission is represented by a thick red cross. The dashed circle gives a rough size of the field-of-view of the radio imaging with radio sources outside this circle not represented by the derived source position and size. The thick magenta circles give the flare-averaged 2.2 MeV gamma-ray footpoint locations (from Hurford et al. 2006) with the circle radius representing the 1σ uncertainty in the source location.

A second example of correlated gamma-ray and sub-mm emission is given by Silva et al. (2007) for the 2 Nov. 2003 flare. Unfortunately, because of the large absolute uncertainty in the radio positions, it was not possible to determine whether the sub-mm source was located at the 200-300 keV footpoints or at the 12-25 keV looptop seen with RHESSI. Nevertheless, Silva et al. (2007) conclude that the most likely source of the sub-mm emission "is gyrosynchrotron radiation from nonthermal electrons, but even this explanation may require adopting high local magnetic fields, very large densities of accelerated electrons, and very small source sizes, considering that the same number of electrons produce the X rays and sub-mm and microwave radiation."

We are currently coordinating future observations that will also include ALMA (Atacama Large Millimeter Array).

Giménez de Castro et al. 2009, ApJ, 507, 433
Fleishman & Kontar, 2010, ApJ, 709, L127.
Hurford at al., 2006, ApJ 644, L93.
Kaufmann et al, 2004, ApJ, 603, 121
Kaufmann et al., 2009, Solar Phys., 255, 131
Luethi et al., 2004, AA, 415, 1123
Silva et al. 2007, Solar Phys. 245, 311
Trottet et al. 2008, ApJ, 678, 509

2.1.6 **Microflares**

Parker (1988) proposed that microflares/nanoflares occurring quasi-continuously over the solar disk could heat the corona. The viability of this mechanism depends on sufficient integrated energy input rate of these events and on their ubiquity, particularly in the absence of sunspots. Their integrated energy depends on two factors: their occurrence frequency and the total energy input per event, which is highly dependent on the cutoff to the steep nonthermal electron spectrum.

With its attenuators out, RHESSI has uniquely high sensitivity in the energy range from ~3 to 15 keV, and in the first five years over ~25,000 microflares were observed with sufficient counts to be imaged (Christe et al., 2008; Hannah et al, 2008a). All these events were found to be located in active regions (Fig. 2.1.6-1 right). It was found that microflares are not necessarily spatially small, with no correlation between the observed thermal loop size and flare magnitude. Furthermore, the microflare energy in non-thermal electrons was larger than expected because they typically have steep power-law spectra and low cutoff energy. These observations confirm the strong similarity between microflares and much larger flares. Figure 2.1.6-1 (left) plots the frequency of occurrence of microflares vs their energy content, determined with RHESSI. It appears that microflares are too intermittent in both space and time, and their total energy input rate was too small, for the heating of the general corona, but large enough to be significant for non-flaring active-region loop structures in active regions.

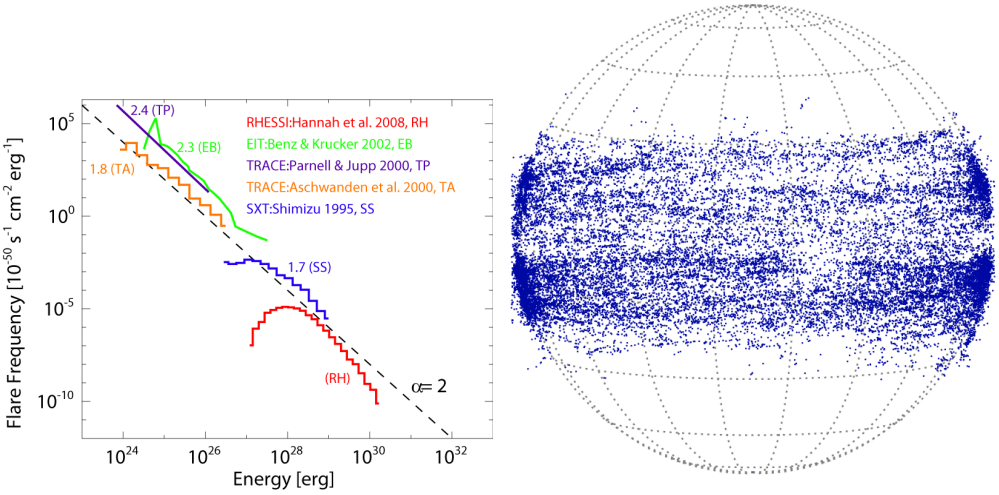

Figure 2.1.6-1. Left: RHESSI thermal energy distribution of microflares (Hannah et al. 2008a). The peak thermal energy for the RHESSI microflares is shown in comparison to the thermal energy distributions found for soft X-ray active region transient brightenings and EUV nanoflares with EIT and TRACE. Right: locations of ~25,000 microflares observed by RHESSI during its first five years of operation from 2002 through to 2007.

Fig. 2.1.6-1 (right) shows that many flares are located just above the limb. Taking advantage of this large statistical dataset provided by RHESSI, Christe et al. (2009) determined that the height distribution of microflares follow an exponential distribution with a scale height of 2.1 Mm and a minimum height of 3.1 Mm above the photosphere. (Note that RHESSI's high angular resolution is precise at the sub-arcsecond level for centroiding, even for weak events.) Comparing with previously published loop length measurements gives an average loop tilt of 44° measured from the vertical.

Christe S. et al. 2008, ApJ, 677, 1385
Christe S et al 2009, AAS/SPD, 40, #19.03
Hannah I.G., et al. 2008a, ApJ, 677, 704
Parker, E. N. 1988, ApJ 372, 719.

2.1.6.1 **Individual Microflare Studies**

Fig. 2.1.6-2 shows a microflare whose non-thermal footpoints (extending up to a surprisingly high ~50 keV) imaged by RHESSI matched spatially and temporally with footpoint emission in soft X-rays (from Hinode/XRT) and EUV (from TRACE). Unlike normal flares, however, the time-integrated HXR emission, however, does not match the soft X-ray temporal profile (e.g., no Neupert effect).

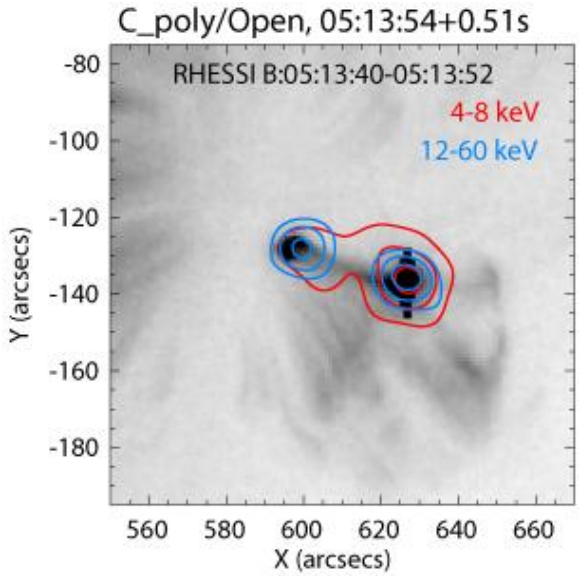

Figure 2.1.6-2. An example of a RHESSI microflare. The blue footpoint contours show nonthermal energy deposition; red contours show the outline of the coronal loop system, seen as well in the Hinode/XRT background image.

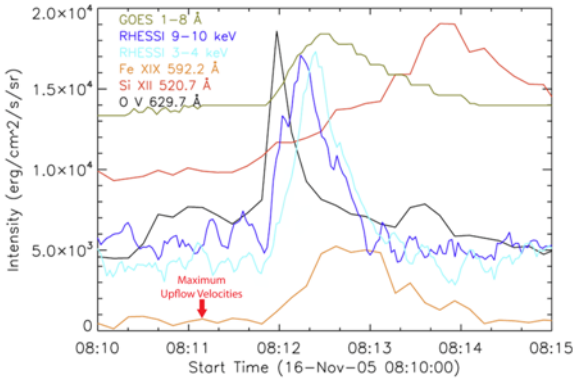

Figure 2.1.6-3. Light curves for various energy bands and spectral lines sensitive to different plasma temperatures for the microflare studied by Brosius & Holman (2009). The red arrow marks the time when He I and O V upflow velocities were greatest.

Not all microflares show evidence of emission from nonthermal electrons, however. Brosius & Holman (2009) used RHESSI observations along with rapid-cadence EUV spectra from SOHO CDS to study the thermal emission from a microflare on 16 November 2005. They determined that this flare exhibited the characteristics of gentle chromospheric evaporation with the RHESSI X-ray emission, centered about 7″ from the centroid of the EUV source, peaking over a minute after the maximum upflows seen in the chromosphere and transition region (Figure 2.1.6-3). RHESSI detected the hottest plasma in the microflare, but showed no evidence for emission from nonthermal electrons.

Brosius, T. and Holman, G. D. 2009, ApJ 692, 492-501
Hannah I.G. et al., 2008b A&A, 408, L45

2.1.6.2 HXR emission from type III solar radio bursts

RHESSI detected very weak hard X-ray (HXR) (12-15 keV) bursts accompanying each of six interplanetary type III radio bursts occurring in a 12 minute interval (Christe et al (2008). The radio bursts are observed up to 150 MHz with some up to 600 MHz. Simultaneous observations by TRACE show jetlike eruptions emanating from the region of HXR emission. The observed HXRs, however, were inconsistent with emission from the escaping type III-producing electrons. Instead, the type III acceleration process appears to be associated with an explosive release of $<\sim 5\times10^{26}$ ergs in the form of a ``superhot" (26 MK) thermal plasma in the corona, an energy comparable to that associated with the type III-producing electrons.

Krucker et al (2008) reported a purely coronal hard X-ray source detected by RHESSI in a partially disk-occulted solar flare that was associated with radio type III burst and a suprathermal electron event detected near 1 AU by the WIND spacecraft. The HXR spectrum, timing and spatial structure are consistent with thin-target emission from the escaping electrons, but the number of electrons detected by WIND are about an order of magnitude too low to produce the observed HXRs. With a simple model Saint-Hilaire et al (2009) showed that only the largest type III burst/electron events could be detected by RHESSI in HXRs. One possibility is that wave-particle interactions may significantly modify the spectrum and numbers of the electrons in solar flares and of the electrons escaping to the interplanetary medium (Hannah et al, 2008; Kontar and Reid, 2009).

Christe et al (2008) ApJ, 680, L149
Saint-Hilaire et al (2009) 696, 94
Hannah et al, (2008) 707, L45
Kontar and Reid, (2009) ApJ, 695, L14

2.1.6.3 **The quiet Sun and axions**

During the quietest conditions when no active regions are present, a fan-beam modulation technique (Hannah et al. 2007a) - pointing RHESSI slightly off the solar disk (between 0.4 and 1˚), thus chopping the solar signal as the spacecraft rotates at ~15 rpm - was utilized to allow the faint solar disk to be distinguished from instrumental and terrestrial background. This off-pointing process has been successfully conducted many times since 2005 during periods of quiet Sun when no active regions/sunspots were on the disk. Initial analysis of these observations produced preliminary upper limits to the quiet-Sun X-ray flux between 3 to 200 keV and showed that the 3-6 keV emission from the quiet Sun is at least two orders of magnitude smaller than the smallest microflares observed with RHESSI (Hannah et al. 2007b). The most recent RHESSI limits (from 12.6 days of exposure) are shown in Figure 2.1.8-3(Hannah et al., 2010).

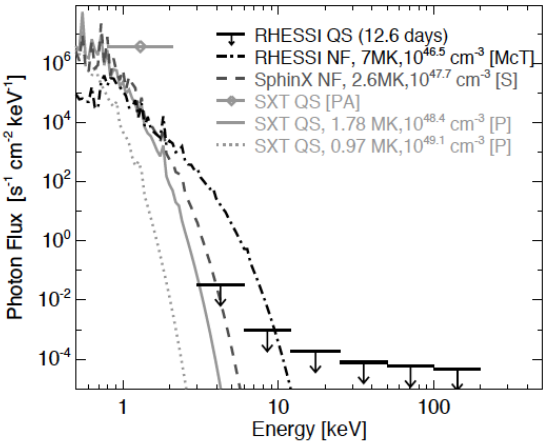

Fig. 2.1.8-3. New RHESSI upper limits on quiet-Sun hard X-ray emission (Hannah et al. 2010), compared with various other determinations as shown in the figure title. These data represent 12.6 days of exposure in the special offpointing mode

The limits of the quiet-Sun emission found with RHESSI have been used to put limits on the coupling constant of the theoretical axion particle (Hannah et al. 2007b). These particles have been postulated to solve the strong-CP problem in quantum chromodynamics and have a cosmological significance as a dark-matter candidate. Axion searches are an active topics of research in fundamental physics and cosmology (see Andriamonje et al. 2007; Irastorza et al. 2010, for details of the ground-based search at CERN). Solar axions should be produced copiously in the Sun's core via nuclear reactions, with the average energy calculated to be 4.2 keV (Van Bibber et al. 1989), and with a narrow ^{57}Fe line near 14 keV (Moriyama 1995). These axions can directly convert to X-ray photons of the same energy in the corona through interactions with magnetic fields perpendicular to their velocity vector. The limits found with RHESSI are comparable to the limits on the axion-photon coupling constant found with the CERN Axion Solar Telescope (CAST) (Andrianonje et al. 2007) for low mass axions.

Andriamonje et al. 2007, JCAP 04
Hannah I.G. et al. 2007a, Rev Sci Inst 78, 024501
Hannah I.G. et al. 2007b ,ApJ 659, L77
Hannah et al. 2010, Sp. Sci. Rev., to be published
Irastorza, I. et al. 2010, J. Phys, 203, 012036
Moriyama, S., 1995, Phys. Rev. Lett. 75, 3222
Van Bibber et al. 1989, Phys Rev D, 39, 2089

2.1.7 **HXR correlations with CMEs**

CME Acceleration & HXR Flux

Given the geoeffectiveness of CMEs, the effort to understand and eventually to predict these powerful solar events has become a major activity of the HP program. As we know, CMEs sometimes occur without flares and vice-versa, but the largest flares tend to be associated with fast and powerful CMEs. Most models of these events include an intimate magnetic connection between the initiation and early acceleration of the CME and the energy release in the associated flare. Temmer et al. (2008, 2010) studied three fast CMEs seen close to the limb with STEREO/EUVI and COR1 and obtained the full CME kinematics of the impulsive acceleration phase up to ~4 $R_\odot$ is measured with a high time cadence of 2.5 min. They find that the CME acceleration profile and the flare energy release as evidenced in the RHESSI hard X-ray flux evolve in a highly synchronized manner (Fig. 2.1.7-1) for all three events studied, consistent with magnetic reconnection occurring in a current sheet behind the CME, as envisaged in the standard flare/CME picture..

On the one hand, magnetic reconnection adds poloidal flux to the CME sustaining the Lorentz force which drives the CME acceleration. On the other hand, the higher the acceleration of the CME, the larger the space that is evacuated per unit time in the coronal region behind it, allowing external magnetic pressure to drive a stronger mass inflow into the reconnection region, which, in turn, causes stronger magnetic reconnection in the current sheet beneath, i.e., stronger flare energy release.

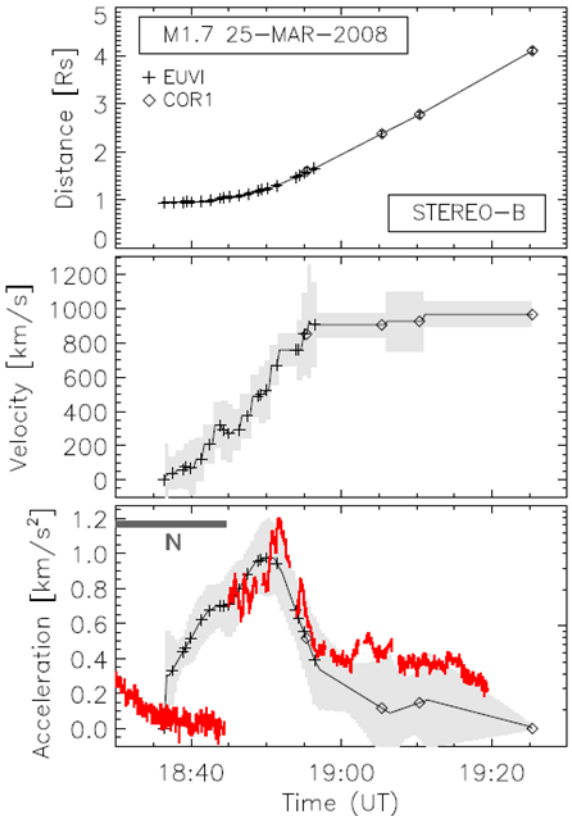

Figure 2.1.7-1: CME kinematics of the 2008 March 25 M1.7 flare/CME event Top to bottom: CME distance, velocity, and acceleration against time together with the background-subtracted flare HXR flux (red, log scale). The gray bar with the letter 'N' indicates the time range of RHESSI night.

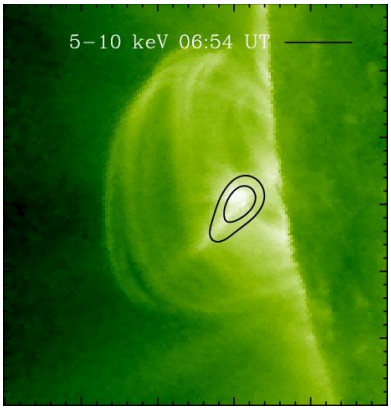

Figure 2.1.7-2. Stereo-B EUVI image of event on 25 Jan. 2007 showing bright emission above the limb with RHESSI 5-10 keV contours overlaid.

Temmer, M. et al., 2008,ApJ, 673, 95.
Temmer, M. et al. 2010, ApJ, in press
(arXiv:1002.3080v1)

Current sheet in CME wake

Coordinated X-ray and EUV observations also allow for a thorough investigation of the intimate connection between flares and CMEs, with particular emphasis on X-ray emission along the current sheet related to reconnection during (occulted) eruptive events. Milligan et al. (2010) found evidence from RHESSI observations for enhanced electron acceleration during the collision of a downward-propagating plasmoid seen with STEREO-B EUVI with an underlying looptop (Figure 2.1.7-2). The increased energy release was apparent in HXRs (9 - 18 keV) and radio emission (245 MHz), both of which are evidence of nonthermal particles. The plasmoid itself is evidence for a current sheet tearing in the wake of the erupting CME, which was also observed by STEREO. As the CME accelerated, the plasmoid was observed to decrease in altitude and ultimately collide with the top of the underlying loop system.

Such collisions are rarely observed as most plasmoids tend to rise. (This is the first observed by RHESSI, and only one similar observation was made by Yohkoh). A recent numerical simulation by Barta et al. (2008) suggests that the formation (and propagation) of such plasmoids can reveal significant details of the CME/flare-related current sheet, magnetic reconnection rates, and subsequent energy release. A more detailed spectroscopic analysis of RHESSI data could reveal important information about the acceleration process. Coordinated observations with STEREO can also shed light on how parameters controlling the CME affect the formation of plasmoids in the current sheet where magnetic reconnection takes place.

Barta et al. 2008, A&A, 477, 649.
Milligan et al. 2010, ApJ, in press.

2.1.8 RHESSI observations in visible light

Because of its requirement for sub-arcsecond aspect information, RHESSI has correspondingly precise tools for image alignment. These requirements resulted in a major serendipitous capability for RHESSI to study the Sun at ordinary visible wavelengths, but via methods never possible before. The solar aspect sensor (SAS) consists of three 4-cm simple lenses observing the continuum at 670 nm via linear CCDs, for which the limb profiles (six in all, typically at a rate of 16 sets s^{-1}) provide the instantaneous pointing direction of the RHESSI instrument. This results in a huge amount of data (more than 10^{10} data points in the first 8 years) of great precision. The rotation of the spacecraft permits the measurements of limb shape and photospheric brightness distribution to be made *differentially* and with a high degree of redundancy. All elements of the RHESSI SAS continue to perform flawlessly.

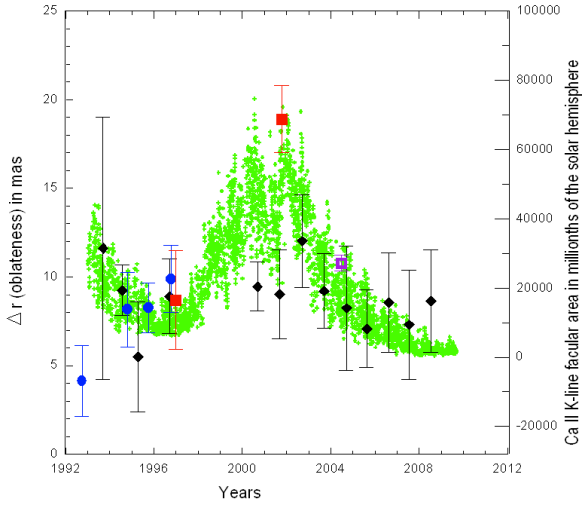

Fig. 2.1.9-1. Time history of recent measures of the solar oblateness, from Rozelot et al. (2010). The RHESSI point is the one with the small error bars in 2004, with the value 10.58 ± 0.44 mas. The other points are as described by Rozelot et al.

Chapman in the 1980s and 90s (e.g. Chapman et al. 1997). The resolution of the debate came when Fivian et al. (2008) found a good correlation between the RHESSI radius determination and the limb brightness in 284Å EIT images. This allowed an empirical correction to be made, with the result shown in Fig. 2.1.9-2, which shows the RHESSI radius measurement as a function of position angle around the solar limb. The red line shows the best-fit oblateness measure without correction for facular contamination. In the right panel we have folded the data into one quadrant and shown how the EIT-based facular correction reduces the oblateness value to nearly that expected: 8.01± 0.14 mas. The success of the EIT masking against faculae (or more generally, magnetic elements in the atmosphere) results from its much greater sensitivity than white-light photometry.

Appourchaux, T. et al. 2010, A&A Rev.18, 197
Chapman, G.A. & Ziegler 1997, Sol. Phys. 168, 259
Dicke, R.H. 1970, ApJ 159, 1
Fivian, M. et al. 2008, Science 322, 560
Fivian, M. et al. 2009, Science 324, 1143-c
Fivian, M. et al. 2010, AAS/SPD abstract
Rozelot, J.P. et al. 2010, JASTP in press

The first scientific application of these data has been to determine the oblateness of the Sun, defined as the excess of the equatorial radius over the polar radius, $(R_{eq}-R_{pol})/R_{eq}$ (Fivian et al. 2008, 2009). This produced an interesting result, as shown in Fig. X1 (from Rozelot et al. 2010, a full review of the subject). The RHESSI measurement, the result of an integration of about three months of data at an intermediate state of solar activity, of 10.58 ± 0.44 mas (milli-arc-sec), is much larger than the Dicke (1970) estimate of 7.98 mas expected from the the rotation of the Sun taken as a uniform value. Note that this error bar, much improved in further analysis, already is much smaller than any of the earlier estimates.

The green points in Fig. 2.1.9-1 show the San Fernando Observatory facular index. The presence of faculae and enhanced network has always been an issue for precise measurements of the shape of the Sun, its limb darkening, and its temperature distribution. This led to a long debate between R.H. Dicke and G.

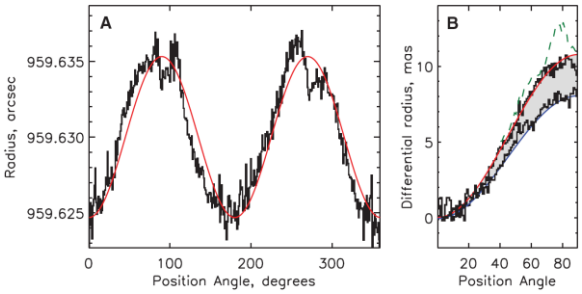

Fig. 2.1.9-2. Dependence of RHESSI radius measures in the 2004 data reduction (Fivian et al. 2008, 2009) as a function of position angle, showing the excellent SNR on the dominant oblateness term. Here 180° and 270° are the W and E limbs, respectively. The right panel shows the same data folded onto one quadrant; the lower curve excludes magnetic elements and thus gives the best view of the purely hydrodynamic solar oblateness

2.1.8 Terrestrial Gamma-ray Flashes (TGFs)

RHESSI was the second spacecraft, after the Compton Gamma-Ray Observatory, to record terrestrial gamma-ray flashes (TGFs) associated with thunderstorms. With no burst trigger (the energy and time of arrival to a microsecond of every photon is telemetered down), RHESSI detected TGFs far more frequently than expected (about 900 TGFs to date), and found that the energy spectrum extended up to ~20 MeV. These findings revitalized the field; now four space missions being prepared for launch over the next few years that include detectors specifically intended for TGF studies: the European TARANIS and ASIM, the Japanese RISING-II (SpriteSat), and the US microsatellite Firefly. Interest in TGFs stems from their possible role in lightning initiation, their possible

connection to other poorly-understood thunderstorm electrical phenomena such as blue jets and sprites, and even a possible radiation health risk to airline passengers (Dwyer et al. 2010). The underlying particle acceleration mechanism thought to be responsible for the energetic emission, relativistic runaway breakdown, is of interest to high-energy solar physicists and astrophysicists as well, since it is related to sub-Dreicer acceleration in plasmas.

Since the last senior review, comprehensive studies of the RHESSI TGF database have surveyed the local time, geomagnetic, and geographical distributions of TGFs, along with the range of variation in duration and spectrum (Grefenstette et al. 2009); studied the spectral variation of the gamma-rays with distance from the spacecraft and to constrain TGF production altitudes and beaming (Hazelton et al. 2009); and examined the relation between TGF occurrences, tropopause height, and storm-development phase (Smith et al. 2010). Research groups studying the radio emission from lightning have done in-depth case studies of RHESSI TGFs, comparing them to the associated discharges, showing that TGFs are associated with intra-cloud lightning and in particular the mysterious, powerful radio signals called Narrow Bipolar Events (NBEs) (Shao et al. 2010, Lu et al. 2010).

Two recently-launched astrophysics missions, Fermi and AGILE, have begun detecting TGFs; positron-beam TGFs have recently been discovered by Fermi. RHESSI's TGF detection rate has dropped because of radiation damage to the germanium detectors, but should be revitalized in the next anneal. In its well-annealed state, RHESSI is still the most sensitive of these instruments to short-duration (< 500μs) and faint TGFs.

Dwyer, J. et al. 2010, JGR, in press.
Grefenstette, B. et al. 2009, JGR, 114, CiteID A02314
Hazelton, B. J. et al. 2009, GRL 36, CiteID L01108
Lu, G.-P. et al. 2010, JGR, submitted.
Shao, X.-M. et al. 2010, JGR, in press.
Smith, D. M. et al. 2010, JGR doi:10.1029/2009JA014853, in press.

2.1.9 Astrophysics Results

Gamma-Ray Bursts (GRBs)

Thanks to its broad energy range and wide field of view, RHESSI has made valuable contributions to the study of astrophysical Gamma Ray Bursts (GRBs). These energetic transients have peak energies ranging from tens to hundreds of keV. Determining this peak energy via spectral fitting helps constrain overall burst energetics and may provide information about its intrinsic luminosity via a variety of empirical correlations. The Swift GRB satellite, which localizes many bursts, is sensitive only to 150 keV, so RHESSI has played a key role in extending spectral coverage of GRBs into the MeV range. Graduate student, E. Bellm (UCB), is continuing the analysis of RHESSI measurements of GRBs for his PhD thesis under the direction of Professor S. Boggs.

2.2 SCIENCE OBJECTIVES for 2011 - 2014

2.2.1 Flare Rates and Energetic Events

We are now slowly emerging from the very long minimum in solar activity as indicated by the increase in the flare rate over the last few months. In early February, an active region (NOAA 11045) produced five M-class flares and 23 C flares in a two-day period. The lightcurves of one of the M flares seen by both RHESSI and GBM on Fermi is shown in Figure 2.2.1-1. This is one of the first large flares seen in common with these two instruments and provides an excellent opportunity for cross calibration. The image overlays shown in figure 2.2.1-2 demonstrate RHESSI's continued imaging spectroscopy capability.

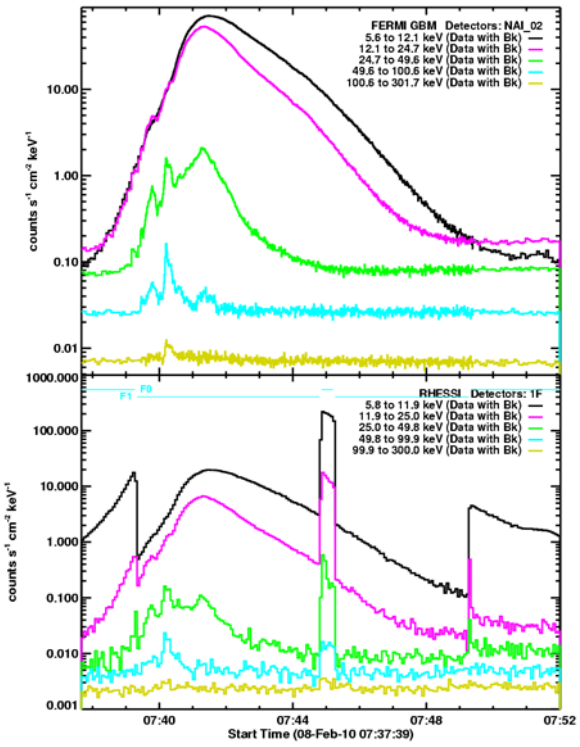

Figure 2.2.1-1 Fermi GBM (top) and RHESSI (bottom) time profiles of the M-class flare on 2010 Feb. 8 with the same nominal energy ranges. Note the possible effects of pulse pile-up in the GBM plot and the shutter transitions in the RHESSI plot.

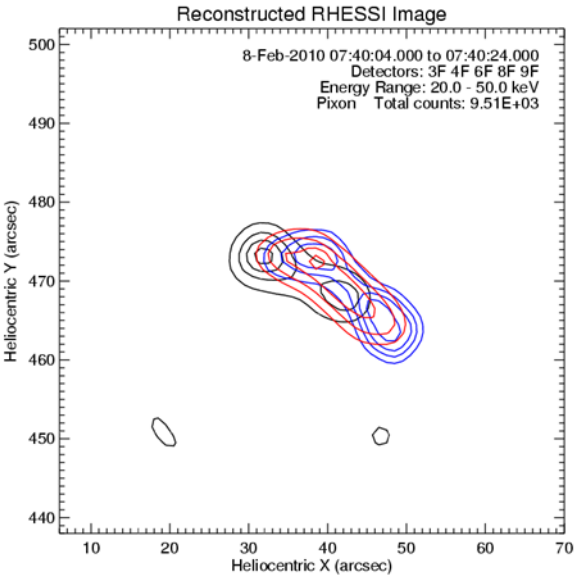

Figure 2.2.1-2. RHESSI photon flux contours at 30, 50, 70, and 90% of the peak fluxes in three different energy bands for a 20 s time interval during the impulsive HXR peak at 07:40 UT. Blue contours: 6 – 10 keV, red: 10-20 keV, black: 20 50 keV.

As pointed out by Temmer (2009) and others, the long duration of the current solar minimum is not unprecedented, and we expect that solar activity will rise rapidly in 2010 towards the next solar maximum. The main question is how intense the cycle will be, and this is addressed in Figure 2.2.1-3, where we have plotted the predicted flare rate based on an average of the rates of X-ray flares seen in over the last three cycles. We believe that RHESSI's unique high-energy measurements will be essential for studies of solar activity, especially flare energy release and particle acceleration. With all the other solar missions (STEREO, Hinode, SoHO, SDO) now observing the Sun in other wavelengths providing crucial context information, we expect to make major advances in our understanding of these key heliophysics processes. RHESSI is the ideal high-energy complement to the high-resolution optical imager and vector magnetograph, soft X-ray imaging, and EUV imaging spectroscopy of Hinode, and the 3-D imaging in EUV and white-light coronagraphy of STEREO and SoHO for studying flares and CME initiation. Highly sensitive energetic electron and ion measurements, separated in longitude, made by STEREO, Wind, and ACE, are perfect for comparisons with RHESSI's sensitive measurements of energetic particles at the Sun. The precise white-light measurements of the solar limb made by RHESSI/SAS continue to provide a unique probe of the fundamental physics of the Sun.

As before, RHESSI will contribute unique measurements for the study of TGFs and cosmic gamma-ray bursts and other high energy astrophysical phenomena.

Temmer, M., 2009, ASP Conference Series, arXiv:1002.0413

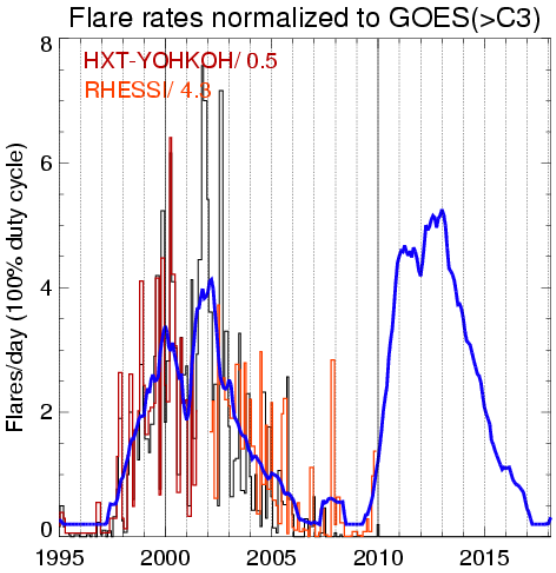

Figure 2.2.1-3. Predicted rates of X-ray flares for the next solar cycle (blue curve) based on the average of the rates from the three previous cycles as measured with other X-ray instruments (ISEE-3, SMM/HXRBS, CGRO/BATSE, and Yohkoh/HXT (Aschwanden, private communication). The black histogram shows the rate of GOES >C3 flares, and the measured rates for the other two instruments (Yohkoh/HXT in red and RHESSI in orange) have been normalized to that rate by dividing by the indicated factors.

2.2.2 Coordination with Fermi

In June 2008, RHESSI was joined in orbit by the *Fermi* Gamma-ray Space Telescope providing a unique opportunity to make simultaneous hard X-ray and gamma-ray observations. The Gamma-ray Burst Monitor (GBM) covers the energy range from ~8 keV to ~40 MeV and the Large Area Telescope (LAT) extends the range up to several hundred GeV. LAT can also provide the centroid source location to within ~30 arcsec above 500 MeV for comparison with RHESSI's gamma-ray images in the 2.223 MeV neutron-capture gamma-ray line. *Fermi* will also detect neutral pions produced in the same reactions as the positive pions that yield positrons responsible for some of the annihilation line emission observed by RHESSI. The high-energy protons can penetrate below the photosphere and may be responsible for the helioseismic waves and recent near-IR observations. Joint high-sensitivity RHESSI and *Fermi* measurements also may detect gamma-rays from delayed CME shock-accelerated particles that may impact the solar atmosphere after the impulsive phase of a flare. Delayed annihilation and neutron-capture line emissions have already been detected by RHESSI following the impulsive HXR phase of the 10 September 2005 flare.

A Fermi GI program (B. R. Dennis, PI) is providing ready on-line access for the solar scientific community to both GBM and LAT flare observations. It allows joint spectral and time-series analysis to be carried out using familiar RHESSI software. An example of this capability is shown in Figure 2.2.1-1 with flare lightcurves for a sunward GBM detector and a single RHESSI detector.

2.2.3 RHESSI Flare Studies with Hinode, STEREO, and SDO

Comparing Hinode, STEREO, SoHO, and SDO observations with the RHESSI data set will greatly enhance the scientific return for all these missions. Only RHESSI provides the key high-energy observations.

Pre-flare physical conditions & flare response

Hinode carries a high-resolution optical telescope (SOT), an EUV imaging spectrograph (EIS), and a soft X-ray telescope (XRT), perfect complements to RHESSI's high-energy observations for studies of solar activity. Hinode/SOT will provide the first stable time-series observations of the solar vector magnetic field, at the highest possible angular resolution. Together with XRT soft X-ray imaging and EIS EUV imaging and spectroscopy, this gives the best information to date regarding the pre-event physical conditions in the solar corona. In some manner not yet understood, these conditions change gradually to a "trigger point", at which time an instability or loss of equilibrium occurs (e.g., Forbes 2000). Arguably the best signs of the initiation are the non-thermal effects, as observed by RHESSI, even in the weakest microflares. The combination of RHESSI and Hinode observations thus will provide our best and most objective determination of the trigger conditions.

Figure 2.2.2-1.shows an example of the richness of data that is now becoming available from EIS. It shows a raster taken during the impulsive phase of a C-class flare. The images show the bright footpoints in the Fe XVI line (formed at 2.5 MK), along with the corresponding Doppler velocity map (derived from line shifts), the nonthermal velocity map (from line broadening), and the electron density map (from line ratios). The overlaid contours on each image show the location of the 20-25 keV sources observed by RHESSI that are assumed to be the footpoint bremsstrahlung emission from the incident high-energy electrons. The EIS data show that these electrons had a significant effect on the ambient target material, heating it to high temperatures and densities, causing it to rise at considerable velocities, and generating turbulence. RHESSI observations play a crucial role in determining the magnitude and location of the energy deposited by the accelerated electrons which ultimately drive chromospheric

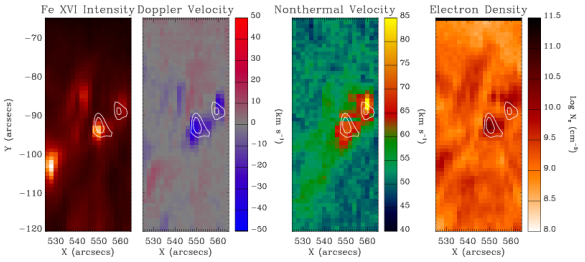

Figure 2.2.2-1. EIS raster taken during the impulsive phase of a C-class flare. Images from the left show Fe XVI intensity and Doppler velocity, nonthermal velocity, and electron density. The same RHESSI 20 – 25 keV HXR contours are overlaid on each image.

flare emission. Future coordinated flare observations between RHESSI and EIS can reveal how changes in the electron distribution (spectral index, low-energy cutoff, and total energy) affect the chromosphere response.

These observations suggest that future, more detailed work, may help us understand the segregation of the elements that we see as the FIP effect, which distinguishes coronal and photospheric abundances and affects both the solar wind and high-energy particles in the heliosphere (the SEPs).

Sunquakes

The arrival of global seismic waves as a manifestation of the flare impulsive phase means that they join Moreton waves, meter-wave type II radio burst shocks, and EIT waves as global consequences of the major flare energy release. All are consistent with an impulsive-phase origin; and the forthcoming Cycle 24 observations, with STEREO, Hinode, and now SDO, will show how all of these signatures are related, and what constraints they place upon the nature of the sunquakes. RHESSI is the only imager operating in the near future that can provide the crucial observations in HXRs and γ-rays.

Coronal Hard X-Ray Sources

We expect a further dramatic increase in our understanding of coronal hard X-ray sources by combining RHESSI observations with Hinode, STEREO, and SDO observations during the upcoming solar maximum. RHESSI can identify the coronal regions, both pre-flare and during the impulsive phase, that appear to be the sites of flare energy release, magnetic reconnection, and electron (and ion) acceleration. XRT will provide the high-cadence high-resolution imaging of these high-temperature regions. EIS imaging spectroscopy can provide the key measurements of flows and turbulence in these regions to clarify the energy release and particle acceleration processes. STEREO/EUVI will provide 3-dimensional observations of flare loops seen in EUV, while SDO will provide the high cadence imaging of flares in multiple wavelengths anywhere on the disk. SDO and Hinode vector magnetograms are the first from space, and they have high resolution. The development of more accurate coronal field models is a major objective that will allow the field evolution during a flare to be compared to different flare models.

Partially Occulted Flares

STEREO observation will provide different view angles of partially occulted flares seen by RHESSI. For at least one of the two STEREO spacecraft, the flare will not be occulted, thus providing information about the magnetic structure. EUV ribbons will give us the likely location of the occulted HXR footpoints. The CME geometry seen with STEREO coronagraphs COR-1/2 can be compared with the HXR coronal source location. RHESSI observations confirm that about 10% of all flares are usefully occulted, i.e. their bright footpoints obscured from view. However, relatively large flares are needed to get good counting statistics, so only a few good candidates will occur until the flare rate increases leading up to the next solar maximum. Thus, in the next few years, we expect that there will be many joint observations of flares that will be disk-occulted from RHESSI, SDO, and Hinode, but that one of the STEREO spacecraft will see on the disk.

2.2.4 *In Situ* Particle Observations and HXR Emission

In 2011-14, as activity increases toward maximum we expect to observe many large flares/SEP events. RHESSI's gamma-ray line measurements of the spectrum of energetic protons and its imaging of the ion source at the Sun can then be compared to the ACE, Wind, and STEREO multi-point SEP spectral measurements spread in longitude,. These comparisons could determine whether solar flares directly contribute to SEPs at 1 AU when the flare is magnetically well connected, as suggested by the 20 Jan 05 event (Section 2.1.5.2).

With many more (and more intense) impulsive electron events detected at 1 AU near solar maximum, RHESSI will have an excellent chance to detect the thin-target emission from the escaping electron beams that produce type III radio bursts. STEREO will provide 3-dimensional event geometry of the solar source region of the escaping electrons and STEREO/WAVES will track escaping electrons by their radio emission. Although the RHESSI observations are only 2-dimensional images, the relatively simple source structure in X-rays (footpoints) will make it possible to put the X-ray emission in the 3-dimensional geometry.

The STEREO IMPACT suite, the SupraThermal Electron (STE) and Solar Electron Proton Telescopes (SEPT) instruments, and the Wind 3D Plasma & Energetic particle instruments will measure impulsive electron events from ~2 to 300 keV. The two STEREO spacecraft will provide these *in situ* measurements at widely separated solar longitudes. By tracking the electrons from the solar source HXR emission imaged by RHESSI, through the interplanetary medium using the Type III radio emission, to the *in situ* detection by the Wind and STEREO spacecraft, we can trace and study the magnetic connectivity from the Sun to the Earth.

2.2.5 Microflares

Combined microflare observation of RHESSI, STEREO, Hinode, and SDO will allow detailed studies of single microflare events to see if microflares are indeed just smaller version of large flares or whether they are a separate type of event. Hinode/EIS will provide observations of plasma flows, while the combination of Hinode/SOT, XRT, and EUVI will provide 3-dimensional magnetic structure and estimates of flare volumes. RHESSI observations will be an essential part of these studies since it is the only instrument that can provide higher temperature (>20 MK) diagnostics and give quantitative measurements of the energy content in non-thermal electrons. The energetics of small-scale energy release in the solar atmosphere (microflares, "blinkers", flaring bright points, and many other manifestations) may have a strong relationship to the coronal heating problem.

Individual microflares have begun to be analyzed using both RHESSI and Hinode/XRT (Section.2.1.4..2). The next stage is to investigate statistically the properties of microflares observed with RHESSI, SDO, STEREO, and Hinode, to understand the results of the large RHESSI microflare statistics study (Christe et al. 2008, Hannah et al. 2008). These studies revealed an unexpected puzzle: these events have steep nonthermal spectra, and no measureable low-energy cutoff. They thus appear to be substantially more energetic than anticipated. Systematic studies at higher resolution (Hinode) and with detailed photometry (SDO), together with STEREO perspective information, may yield a resolution of this problem, which is essential to our understanding of flare energetics. (Hannah et al. 2010).

Christe S., Hannah I.G., Krucker S. Lin R.P, McTiernan J, 2008, ApJ, 677, 1385.
Hannah I.G., Christe S. , Krucker S. Hurford G.J, Hudson H.S, Lin R.P, 2008, ApJ, 677, 704.
Hannah, I. G. et al., 2010, Space Science Rev., in press

2.2.6 Gamma-Ray Observations

Future work to improve the reconstructed gamma-ray images will be directed along two lines. First, improved analysis techniques based on ***visibilities*** will improve the statistical significance of the results. Second, improved background- and continuum-subtraction techniques (also visibility-based) represent a promising avenue to enable imaging in the 511 keV line. The significance of this is that RHESSI can image such lower energy gamma-ray line photons with much better angular resolution compared to 2.2 MeV photons because the finer but thinner grids give usable modulation at this energy. As solar maximum approaches, more gamma-ray flares will be detected, allowing more systematic studies.

The nuclear de-excitation lines, positron-annihilation line and neutron-capture line in flares can reveal a great deal about accelerated ions -- their composition, spectrum, and angular distribution -- and about the density and composition of the solar atmosphere in which the ions are interacting. The large gamma-ray line flares detected to date by RHESSI have had relatively low line to continuum ratios compared to those detected by SMM. With the increase in the number of such events as activity rises to maximum in 2011-14, we hope to catch some large flares with high line to continuum ratios so the power of high resolution spectroscopy can truly be exploited, and imaging in the prompt de-excitation lines may become feasible.

2.2.7 RHESSI/SAS White Light Observations

Table 2.2.7-1 gives a roadmap to the use of the RHESSI/SAS data, which, in principle, have many applications. The precision of the oblateness result strongly suggests that significant progress will be made in many of these areas. The combination of RHESSI/SAS with SoHO EIT has proven to be a powerful technique to identify weak plage activity. The global oscillations of the Sun (helioseismology) are a natural objective because of the advantage of limb data: the photosphere (e.g. as defined by $\tau_{5000} = 1$, where τ_{5000} is the optical depth at 5000Å) is physically higher at the limb and therefore has larger mode amplitudes. We have already shown the easy detectability of the p-modes (see Figure 2.2.8). The ambition for the longest integration of RHESSI observations is to detect or set meaningful limits on the amplitudes of the g-modes; these modes are trapped in the radiative core of the solar interior and would have very small amplitudes at the photosphere because of their evanescence in the convection zone (e.g. Appourchaux et al. 2010).. Their detection would be extremely significant because of the

direct information their frequencies provide about the innermost core. Because there are g-modes with periods greater than the RHESSI orbital period of ~96 min, the RHESSI analysis will not be complicated by aliased power.

The current efforts center instead on other items in Table 2.1.11-1, specifically the refining the oblateness measurement in terms of time-series results and higher order terms. As a part of this our analysis aims also at using the full 1D images of the Sun obtained by the RHESSI/SAS imagers to determine the global temperature distribution. This is directly important for the oblateness and shape measurements because of the potential for confusion between radius and brightness (limb darkening function).

Table 2.2.7-1: Phenomena accessible (and detected) with precise solar radius measurements.

Magnetic Phenomena		**Hydrodynamic Phenomena**	
sunspots	detected	p-modes	measured
Wilson depression	detected	g-modes	
faculae	detected	r-modes	
active network	detected	granulation	detected
Flares		other convective motions	detected
prominences		oblateness	Fivian et al. 2008, 2009
coronal holes		oblateness time variations	detected
Dynamo signatures		Higher order shape terms	
		Gravitational moments J2, J4	
		Global temperature variation	Fivian et al. 2010
		Planetary tides	

Appourchaux, T. et al. 2010, A&A Rev.18, 197
Fivian, M. et al. 2008, Science 322, 560
Fivian, M. et al. 2009, Science 324, 1143-c
Fivian, M. et al. 2010, AAS/SPD abstract

2.2.8 Terrestrial Gamma-ray Flashes

We expect the collaborative research projects which correlate RHESSI TGF data to radio atmospherics from lightning, optical emission from sprites and elves seen with ISUAL on FORMOSAT-2, and even infra-sound from sprites, to be supplemented by collaborations with the new missions such as Fermi, RBSP, the European TARANIS and ASIM, the Japanese RISING-II (SpriteSat), and the US microsatellites Firefly, Firebird, and CINEMA. RHESSI TGF times and locations are made publicly available in near realtime.

The cosmic gamma-ray burst and other transient studies will continue to exploit the unique timing, spectral resolution, and broad energy coverage of RHESSI. We plan to revisit the Crab for about one week annually at the Sun's closest approach each June. The Crab observations also provide an invaluable absolute calibration of the detector front-segment X-ray sensitivities. In addition, we will continue to image the Crab Nebula and work on improving the aspect solution (the key to obtaining groundbreaking maps) for those solar off-pointings. The inner features of the Crab Nebula are extremely dynamic, showing significant variations from season to season in the optical (HST) and soft X-ray (Chandra) bands (Hester, J. J. et al. 2002).

Hester, J. J. et al. 2002, ApJ 577, L49

2.3 Potential for Performance during FY-11 to FY-14

2.3.1 Relevance to Heliophysics Research Objectives

RHESSI is directly relevant to achieving NASA's strategic goal for Heliophysics to "Understand the Sun and its effects on the Earth and the solar system." It addresses the SMD Science Question - "How and why does the Sun vary?" and the following Research Objectives:

- Understand the fundamental physical processes of the space environment from the Sun to Earth.
- Develop the capability to predict the extreme and dynamic conditions in space in order to maximize the safety and productivity of human and robotic explorers.

2.3.2 Impact of Scientific Results

RHESSI scientific results have been presented at innumerable scientific meetings and published in over 800 papers listed at the following web site:

http://www.lmsal.com/~aschwand/publications/rhessi.html

Many of them are available electronically in the E-Print archive at the Max Millennium web site -

http://solar.physics.montana.edu/max_millennium/

Over 35 PhD and masters degrees that include significant analysis of RHESSI observations have been awarded to date or are in preparation –

http://www.lmsal.com/~aschwand/publications/rhessi_phd.html

2.3.3 Spacecraft and Instrument Health

See Section 3.

2.3.4 Productivity, and Vitality of Science Team

RHESSI personnel have initiated, organized, and attended many scientific meetings and special sessions. In the last three years, the series of international RHESSI workshops continued with events in Potsdam, Germany (Sept. 2008), and Genoa, Italy (September 2009). Each workshop was attended by some 50-60 scientists. RHESSI team members organized the collaborative conference entitled "Solar Activity during the Onset of Solar Cycle 24" in Napa, CA, in December 2008. Several international teams of scientists have met in Bern, Switzerland, under the sponsorship of the International Space Science Institute, to explore issues related to RHESSI's hard X-ray spectroscopy and imaging spectroscopy, for example.

Scientists who have attended the RHESSI workshops are preparing a series of papers for a complete ~500-page volume of Space Science Reviews detailing the current state of understanding of all aspects of high-energy solar flares. The chapter titles (with the lead authors in brackets) are as follows:

- Introduction (Dennis, Emslie)An Observational Overview of Flares (Fletcher),
- Interpretation of Thermal and Nonthermal Electron Distributions (Holman),
- Ion Acceleration and Interaction (Vilmer),
- Correlative Radio and Hard X-Ray Observations (White),
- A Statistical Study of Flare Parameters (Hannah),
- Deducing Electron Properties from Hard X-Ray Observations (Kontar),
- Theoretical Implications (Zharkova).
- Summary & Future (Lin)

Each paper will be published on line as it completes the Space Science Reviews refereeing process. The joint publication of all the papers in book form is expected in the summer of 2010.

RHESSI team members have organized special sessions on high-energy solar physics topics at every meeting of the AAS/SPD since launch and at COSPAR General Assemblies. The latest was organized by CoI, Gordon Holman, at the Montreal COSPAR meeting in July, 2008, and the next one is being organized by Alexander Warmuth in Bremen, Germany, in 2010. In addition, the RHESSI team has held a series of workshops to educate the scientific community on how to use the RHESSI data analysis software in order to obtain the best possible images and spectra.

2.3.4.1 Science Nuggets

Beginning in March 2005, RHESSI team members began putting a biweekly series of "science nuggets" on the following web site:

http://sprg.ssl.berkeley.edu/~tohban/nuggets/

Each nugget is a brief report that is intended to introduce various aspects of the scientific material to a technically competent audience. The wiki format allows us to include images, movies, and links. At the time of writing (March, 2010) there are 122 nuggets online with over 50 different authors. The Webmaster is Steven Christe and CoI Hugh Hudson serves as general editor and default writer in case of schedule gaps. The Nuggets are announced in community newsletters that go to an audience of about 500. Email feedback shows a readership that is both within and outside the solar physics community.

2.3.5 Future Promise

RHESSI is still fully operational and shows tremendous promise for the coming years of increasing solar activity and joint observations with the newer solar missions now in orbit. RHESSI continues to be the only mission capable of solar HXR imaging spectroscopy and is likely to retain that unique position until the launch of the Spectrometer Telescope for Imaging X-rays (STIX) on the European Solar Orbiter in 2017-18. RHESSI's gamma-ray imaging spectroscopy capabilities are unlikely to be matched for many years. Thus, it is critical that RHESSI be available for as long as possible to provide the high-energy coverage of the flares that will be seen in increasing numbers with the new and advanced instrumentation on Hinode, STEREO, SDO, and *Fermi*.

The successful anneal in November 2007 resulted in the recovery of high energy resolution and sensitive volume in the germanium detectors. Tthe effects of radiation damage are building up again, as expected, although RHESSI is still operational. We plan to anneal again once solar activity picks up, and then will be ready to make optimal observations of X-rays and gamma-rays for at least two more years. Additional anneals will be done as necessary.. Ground tests with a spare germanium detector indicate that at least three additional anneals of the same duration and temperature as the one already completed can be safely carried out without endangering the detector segmentation. The cryocooler, while showing signs of degrading performance, is still maintaining the detectors at the acceptable temperature of <100 K with an input power of 70 watts and negligible microphonics.

2.3.6 Data Accessibility and Usability

Full details of RHESSI data accessibility and usability are given in the accompanying Mission Archive Plan. The data archive contains the full Level-0 telemetry data, the RHESSI flare list, and a number of 'quicklook products' including prepared lightcurves, spectra, and images, and summaries of housekeeping data for the entire mission. The archive, currently ~4.5 TB, resides on three servers, at SSL, Goddard, and at ETH in Zurich, Switzerland. It is online, available, and easily accessible by anyone with an Internet connection. The complete RHESSI software package necessary for the analysis of all RHESSI data is also freely available online as part of the Solar Software (SSW) tree. It is mostly written in the Interactive Data Language (IDL licensed from ITT Visual Data Solutions) and is fully compatible with both UNIX and Windows operating systems.. It contains all procedures necessary to read and unpack the FITS data files, prepare and plot light curves, reconstruct images, and accumulate, display, and analyze spectra. For the expert analyst, the procedures can all be invoked from the IDL command line, but a more user-friendly graphical user interface is also available capable of carrying out all the basic analysis tasks.

There is extensive documentation online at the RHESSI web site –

http://hesperia.gsfc.nasa.gov/rhessidatacenter/

Descriptions are available of the mission, the instrument, the science objectives, data analysis techniques, the software, and the data archive. In addition, there are support personnel at all three data sites to guide scientists in using the software and interpreting the results.

2.3.6.1 Browser

To allow for quick inspection of the RHESSI data, there are many automatic routines to produce plots such as quicklook lightcurves and images and detector monitor rates. Navigating this wealth of automatically generated plots is accomplished using a web-based data browser, simply called Browser, found at:

http://sprg.ssl.berkeley.edu/~tohban/browser/

Browser is a powerful tool that allows the user to load a variety of plots relevant for a specified time, and then easily step back and forth through time as desired. It provides the capability of storing the current view as a URL for ease of sharing among researchers. Browser dynamically generates links to non-RHESSI web-based databases (such as magnetograms) corresponding to the specified time so that the user can investigate the context of the RHESSI data. Plans are currently underway to add a link to the Fermi/GBM HXR lightcurves.

2.3.6.2 Facilities for Multi-wavelength Analysis

To achieve the full scientific potential of RHESSI data and to support the convenient integration of RHESSI data into studies initiated in other wavelength regimes, it is essential to have convenient access both to the data from other instruments and to the relevant software resources. Two steps have been taken to ensure this. First, the RHESSI software package includes flexible tools for accessing and integrating multiple data sets (for example by overlaying images). Coalignment is simplified since the absolute positions of RHESSI images are inherently determined to arcsecond accuracy.

Second, we have established a comprehensive RHESSI Synoptic Data Archive at the GSFC Solar Data Analysis Center (SDAC) that allows ready access to a broad range of observations for all the RHESSI flares. The archive contains images, spectra, and lightcurves from a wide range of different instruments, both space and ground-based, stored in standard formats for direct comparison with RHESSI data. The sources include SOHO (EIT and MDI), TRACE, Big Bear Solar Observatory, Kanzelhohe, and Kiepenheuer Hα full-disk images; GOES-12 SXI full-Sun images and GOES 6-12 two-channel light curves with 3 s time resolution; and Phoenix, Owens Valley Solar Array, Nobeyama, and Nancay radio images and spectra.

We are continuously improving the Synoptic archive as follows:

- Increasing the cadence and time coverage of complementary data to encompass pre- and post-flare phases of GOES and RHESSI-observed events.
- Facilitating access to data from new missions as they become available after launch. We have partnered with the STEREO and Hinode science teams to integrate their data analysis tools into the RHESSI analysis software to permit joint analysis of multi-wavelength observations. We will extend this effort to include next generation data from the Solar Dynamics Observatory (SDO)
- Evolving from a centralized synoptic data archive to a distributed system that is incorporated into the Virtual Solar Observatory (VSO). As part of our project to augment the VSO funded under the Heliophysics Division's VxO program, we have teamed with the SDAC to develop an IDL client interface that directly searches and retrieves VSO datasets. By incorporating this interface into the RHESSI analysis software, we are augmenting the range of different solar observations accessible for joint analysis with RHESSI, while simultaneously extending the data analysis capability of the VSO.

3 TECHNICAL STATUS

3.1 Spacecraft

RHESSI was launched on February 5, 2002, into a circular orbit with an altitude of 600 km and an inclination of 38°, and the first solar flare was observed on February 12, 2002.The observatory continues to function very well after more than 8 years of operations in its present 573 x 551 km orbit. All of its subsystems are fully operational. The solar array power output has declined by only 1.1% since launch, the battery voltage has been stable for the past 2 years, the absolute battery pressure has been stable for the past 3 years, and the differential pressure has been relatively stable for the past 1.5 years. The average spacecraft temperature has increased by only ~1° C since launch. The S-band transceiver still generates a stable output power of 4.9 W with clean BPSK modulation at 4.0 Mbps, and the receiver shows no signs of deterioration in performance. The attitude control system is stable and the command and data handling subsystem shows no signs of degradation.

The CPU experienced six resets since launch. Three of these resets occurred as a result of the very large solar flare in October 2003, two were caused by watchdog timeouts during Absolute Time Sequence (ATS) table loading, and one had an unknown cause. In several cases, resets were commanded from the ground to activate a flight-software patch for non-solar observations in off-pointing attitude control mode. The IDPU never reset autonomously, but was reset once by ground command. On two occasions ATS table loads with faulty checksums were erroneously accepted by the spacecraft. However, these ATS tables were subsequently reloaded and verified flawlessly prior to their on-board execution.

Overall, there is no reason to believe that the spacecraft will not continue to function very well over the next three years. The solar arrays have shown minimal degradation and are projected to be capable of providing adequate power for the next three years and beyond. The battery showed some degradation early in the mission, but has been stable for the past two years and is projected to provide adequate power storage for the next years. Generally, the telecommunications subsystem has been stable since launch. However, following the detector annealing in November 2007, the receiver appears to be seeing excessive noise from the bus due to higher power consumption by the cryocooler. As a result, ATS table loads became unsuccessful during nighttime passes. This situation is easily mitigated by scheduling daylight passes at the Santiago ground station during infrequent periods in the year when both the Berkeley and Wallops ground stations have nighttime passes only. Aside from this problem, all other subsystems and sensors are functioning nominally.

3.2 Instruments

3.2.1 Spectrometer and Cryocooler

The RHESSI germanium spectrometer and its Sunpower cryocooler continue to work well. The cooler has operated nearly continuously for more than 70,000 hours - at its standard constant-amplitude mode at ~65 watts from the first week of the mission to up to the detector anneal process done in November 2007, and since the anneal at ~75 watts to maintain the coldplate temperature at between 90 and 100 K. With the cryocooler operating in its standard constant-amplitude mode, the temperature of the detectors fluctuates 3-5 K while the orbital eclipse period varies. For reasons that are still inconclusive, the cooling performance gradually declined, with the coldplate temperature increasing from an initial value of ~70 K to ~90 K just prior to the anneal. Two thirds of the rise in temperature occurred over the first two years of operation, stabilizing when the spectrometer's insulating vacuum volume was vented to space on February 5, 2004. By implication, there was probably condensable contamination in the spectrometer vacuum volume causing degradation of its thermal performance. Opening the vent probably stopped further accumulation of condensables, but did not release anything already deposited on the spectrometer's interior thermal surfaces.

The cooler has been used twice to cool down the spectrometer detectors and cold plate from room temperature, on the initial cool down and after the anneal cycle in November, 2007. The cryocooler was kept powered on at ~50 W during the anneal process to keep its own components cool and to prevent damage from excess heat. However, it was operated during that time at an input power that was higher than its design capability at the actual temperatures reached, and it appears that it may have suffered some degradation in performance as a result. For subsequent anneals, the cryocooler will be operated at a lower power setting when the cold-tip temperature is elevated, more closely matching the profile used successfully during initial cool down after launch. The cryocooler performance has stabilized since the anneal, and the cold plate temperature is being maintained at between 90 and 95 K after increasing the input power to 75 watts.

3.2.2 Detector Annealing

The RHESSI germanium spectrometer continues to work well in all respects except for the predicted effects of radiation damage on the energy resolution and active volume of the detectors. This damage can be significantly reduced by annealing the detectors at a temperature of ~90° C for ~7 days, as was done once already in November 2007. We have been waiting for solar activity to recover from the extended minimum before annealing a second time so that the instrument will have the best possible performance as solar activity increases towards maximum.

Annealing is most important for the detection of nuclear lines at high energies. The effect of radiation damage on the detected line shape is due to trapping of holes in disordered regions in the germanium lattice. Although the Gaussian energy resolution after annealing is not as good as the undamaged crystal, the tailing is virtually eliminated. The only two solar lines that are intrinsically narrower than this resolution are at 511 keV (the positron annihilation line) and 2.223 MeV (the neutron capture line). The nuclear de-excitation lines are broadened by Doppler effects, and the annealed instrumental resolution is narrower than the true line shapes.

The largest X-class flares that produce detectable nuclear emission are not usually seen at the beginning of the cycle. The second anneal will give us ~2 years of good gamma-ray line spectroscopy, so we want to time that interval optimally. Based on gamma-ray flare occurrence in previous solar cycles, it appears best to wait for the first active region producing gamma-ray flares (> 300 keV) before a second anneal is carried out, probably in late 2010-2011, as solar maximum approaches.

Severe radiation damage (the pre-anneal state) also leaves a fraction of the detector volume near the outer surface entirely passive (insensitive to energy deposition), reducing the effective area. Annealing also reverses this aspect of radiation damage. By mid-2007, many front segments had lost effective area due to radiation damage, particularly detector #5. Analysis of the X-ray count-rate spectra for three C-class flares detected in 2005, 2007 - pre-anneal, and 2007 post-anneal shows that most of this loss has been recovered by the anneal. Accurate knowledge of the relative sensitivity of the nine RHESSI detectors is important for image reconstruction and for spectral analysis using individual detectors. Knowledge of the absolute sensitivity is important for any comparison with results from other instruments, and is particularly critical in any differential emission measure analysis as evidenced in the comparison of RHESSI and Hinode observations of non-flaring active regions (Reale et al. 2009, Schmelz et al. 2009). We have obtained measurements of the long-term decrease in sensitivity of the front detector segments in the energy range from 6 to 20 keV. We determined both the sensitivity relative to RHESSI's detector #1, which is the most stable of all the nine detectors, and the sensitivity of detector #1 relative to that of the GOES SXR

detectors, which are thought to be quite stable. We will continue to refine these detector sensitivity determinations, adding comparisons with Fermi/GBM spectra as more flares are observed in common. The resulting sensitivities as functions of time will be incorporated in the calibration data files for use in the data analysis routines.

The amount of annealing we can do is limited by the drift of implanted lithium ions at the inner bore of the detectors. The segmentation of the RHESSI GeDs depends on a gap in the inner electrical contact, which is made conductive by the lithium. At high temperatures, the lithium becomes mobile in the Ge crystal and can drift so as to close the gap. This would de-segment the detector and cause several problems for its performance, but it could still be operated as an unsegmented detector. We have repeatedly annealed a spare detector in the laboratory, and it began to de-segment after approximately one month at 95^{o}C. We are therefore confident that a second anneal of 1 to 2 weeks will be possible without de-segmenting the flight detectors.

Reale, F.; McTiernan, J. M.; Testa, P., 2009, ApJ. 704 L58.
Schmelz, J. T. et al.. 2009, ApJ. 704, 863.

3.2.3 Imager

The RHESSI imager subsystem consists of nine rotating modulation collimators, each of which has a pair of widely separated grids. A metering structure maintains the relative twist alignment of the nine grid pairs. The imaging subsystem is inherently stable and has shown no evidence of change in grid alignment. Improved analysis techniques are refining the calibration of the grid parameters and locations (now known to submicron accuracy), the results of which are built into the software package and are applicable to all data acquired since launch.

3.2.4 Aspect System

There are three parts to the RHESSI aspect system. The absolute pitch and yaw angles relative to Sun center are provided by the Solar Aspect System (SAS), with sub-arcsecond accuracy. The spacecraft roll angle is provided by two redundant side-looking star scanners, a CCD-based Roll Angle System (RAS) and a Photomultiplier-Tube-based Roll Angle System (PMTRAS).

The SAS consists of a set of 3 identical lens/sensor subsystems each of which focuses a narrow-bandwidth image of the solar disk onto a linear CCD array. No anomalies in its operation have been observed. During the first few months of the mission, the sensitivity of the SAS decreased, but it has now stabilized at ~60% of the original value, a level which provides an order of magnitude of sensitivity margin with no compromise in accuracy. The SAS also continues to provide the most accurate radius measurements (to 50 mas) ever made, for the study of global solar applications as discussed in section 2.1.7.

The PMT-RAS continues to provide the roll aspect knowledge upon which most of the solar imaging is based. Its response has remained stable since launch, easily meeting its 1 arcminute roll-angle requirement with a large margin in sensitivity.

The CCD-based RAS has also proven to be stable and able to meet the 1 arcminute roll-angle requirement. CCD-RAS data are used to fill occasional gaps in the PMT-RAS coverage. In addition, by measuring the polar angle as well as the roll angle, the CCD-RAS can provide full aspect information with 10 arcsecond accuracy for non-solar targets such as the Crab nebula and the pulsar A0535+26.

3.3 Software

One of the unique characteristics of RHESSI is that the telemetered data contain detailed information on each detected photon. This provides unprecedented flexibility in that decisions and tradeoffs associated with time resolution, energy resolution, imaging resolution and field of view, etc, can be made *ex post facto*, enabling the analyst to make these decisions in the manner best suited to the scientific objectives and to the characteristics of the event under study. The RHESSI software fully supports this flexibility. Another advantage of this photon-oriented database is that ongoing improvements to the software and instrument calibration can be fully applied retroactively to all the data since the beginning of the mission.

The RHESSI software package is well-developed, robust, and available via SolarSoft. It can be used with the IDL command line, a user-friendly graphical user interface, or scripts for automating user-specific tasks. The software generates images, and spatially-integrated or feature-specific spectra and light curves and provides full support for comparisons with data products from other missions. Recent developments have included the fully-integrated generation and analysis of image cubes as a function of time and/or energy to better support imaging spectroscopy. Many important improvements have been made to the spectral analysis capabilities, and software has

been developed to calculate visibilities and to carry out visibility-based analyses. The gamma-ray detector response has also been modified to better account for Compton-scattered photons in the detectors.

Visibilities are calibrated, 'instrument-independent,' Fourier components of the source image. Mathematically, they correspond to the output of a single baseline of a radio interferometer. For RHESSI, they represent an intermediate data product directly obtained from the observed time-modulated light curves. Visibility measurements have well-defined statistical errors. Their value lies in the fact that they depend linearly both on the data and on the source. Consequently, they can be flexibly combined for comparison between source models and observations. The basic visibility software implemented to date has enabled the accurate determination of hard X-ray source sizes (useful for example to convert thermal emission measurements to electron densities), and the evaluation of albedo; it was the computational tool of choice in obtaining several of the recent results discussed in section 2. Refinements in the calculation of visibilities and in their use for other applications (such as improved spectral line imaging, albedo analysis, and subsecond time resolution studies) are priority goals of the ongoing software development effort.

3.4 Ground System

In 1999, a multi-mission operations facility was established at SSL to support the RHESSI and FAST missions. The joint facility, which now also supports THEMIS operations, includes the Mission Operations Center (MOC), the Science Operations Center (SOC), the Flight Dynamics Center (FDC), and the Berkeley Ground Station (BGS). A high degree of integration and automation combined with flexible system architecture provides a reliable and cost effective state-of-the-art environment to perform all functions required to operate multiple spacecraft simultaneously.

3.4.1 Ground Stations

The primary ground station for the RHESSI mission is BGS. Backup support is provided by the Wallops Island (WGS), Santiago (AGO), Merritt Island (MILA), and the DLR ground station at Weilheim, Germany. BGS has supported more than 12,000 RHESSI passes since launch - on average 5-6 passes per day. WGS, AGO and MILA support typically 4 passes per day combined. The average daily data volume is 13.5 Gbits with an overall telemetry recovery efficiency of ~99%.

The BGS consists of an 11-m parabolic reflector mounted on a pedestal with a three-axis drive system, and an S-band RF system. Since the azimuth and elevation gear boxes were rebuilt after a failure in 2002, BGS operations have been very reliable, supporting more than 21,000 passes for RHESSI, FAST, CHIPS and THEMIS combined.

3.4.2 Mission Operations Center

The RHESSI Mission Operations Center is part of a secure, shared state-of-the-art facility with a network of workstations for flight dynamics, spacecraft command and control, mission planning, command load generation, and data trending. The facility, typically staffed during normal working hours only, performs automated pass supports, spacecraft and instrument state-of-health checks, and generation of all ephemeris and planning products in a lights-out mode.

RHESSI normal operations comprise mission planning functions, command load generation, real-time pass supports, spacecraft state-of-health monitoring, data trending, instrument configuration, and science data recovery and archiving. Generation of all ephemeris and mission planning products is based on two-line element sets that are downloaded from the Space-Track.org web site, quality checked and archived locally in a fully automated mode. Spacecraft ATS loads are built by the FOT and uploaded to the spacecraft multiple times per week. Every six weeks, the spacecraft is re-spun from about 14.5 rpm to its nominal spin rate of 15 rpm. The FOT works closely with project scientists to determine the optimal instrument configuration consistent with the current level of solar activity.

During off-hours, FOT members are automatically notified by cell phone regarding any spacecraft or ground system anomalies. A number of web-based tools allow FOT members, subsystem engineers, and instrument scientists to monitor spacecraft and instrument performance remotely.

Since RHESSI is operated from a multi-mission facility, its resources are shared with other missions. This approach provides redundancy and reduces overall operations costs. The flight control team now operates RHESSI and the 5-spacecraft THEMIS for a total of 6 spacecraft. Present planning is for this facility to operate the NuSTAR SMEX mission and the NSF cubesat CINEMA when they are launched in 2011.

3.4.3 Science Operations Center

The RHESSI SOC, located at SSL, consists of a RAID server, with ~13.7 Tbytes of data capacity, and six processors. The SOC receives RHESSI data after every ground-station contact and automatically processes them to create Level-0 data files. As of March 2010, there are ~69,000 Level-0 files, containing 5 Tbytes of data, for an average of 1.8 Gbytes per day.

Other automated procedures generate quick-look data containing the RHESSI observing summary, flare list, and quick-look light curves, images, and spectra. Long-term trend plots of SOH data are updated daily in the SOC. All of these data products are available through the RHESSI Data Center website at Goddard -

http://hesperia.gsfc.nasa.gov/rhessidatacenter/

3.4.4 Max Millennium Program

The RHESSI PI team created and supports the Max Millennium program for several functions that are key to the successful acquisition of observationally complete datasets and the full scientific exploitation of those observations. These functions are accessible at

http://solar.physics.montana.edu/max_millennium/

They include the following:

1. Joint observing plans between RHESSI and other instrumentation with specific scientific goals.
2. Daily observing targets generated each day by one of four experienced solar observers (the Max Millennium Chief Observers)
3. RHESSI data analysis projects submitted by active scientists interested in collaborations.
4. RHESSI software and hardware updates.
5. The Solar Physics E-Print Archive. A recent study indicates that papers in this archive are cited about twice as often as average.
6. Majordomo email for items of interest going to 353 self-subscribed participants.

4 APPENDICES

4.1 Education and Public Outreach

4.1.1 Berkeley

RHESSI: The Heliophysics Educator Ambassadors (HEA) Program

Lead Senior Review Mission: THEMIS

Senior Review Partners: ARTEMIS, AIM, RHESSI, & TIMED

Additional Partners: IBEX, RBSP & MMS E/PO programs

Introduction

Across SMD, many E/PO efforts from missions, research programs, and the Education Forums are responding to the call for effective support of science educators by conducting ongoing professional development (PD) through workshops, institutes, and short courses at conferences and other venues. In an effort to continue to provide greater coherence, we propose to continue a common long-term PD activity started two years ago within the Heliophysics E/PO community to support a common effort – The Heliophysics Educator Ambassadors (HEA) Program. The THEMIS/ARTEMIS mission has led the HEA Program since October, 2008, with support from the following 2008 Senior Review partners: AIM, RHESSI, TIMED, and Cluster. Two other Heliophysics E/PO efforts–IBEX and MMS–provided additional support. This next stage of the HEA program will be lead by both the non-Sr. Review mission, IBEX, together with THEMIS, and with support from the Senior Review partners: ARTEMIS, AIM, RHESSI, and TIMED. Two other Heliophysics E/PO efforts - MMS and RBSP - will also support this effort. Please see the THEMIS EPO section for detailed information on this proposed effort as well as information on results from the past two years.

In addition to the HEA program, each mission engaged in other events specific to its mission science.

Note that Dr. Bryan Mendez was the lead of the RHESSI E/PO but in Feb., 2010, Dr. Laura Peticolas took over as lead for the RHESSI E/PO efforts.

RHESSI – Specific Activities with HEA and in Addition to HEA

RHESSI participated in the HEA program by supporting teachers at the HEA workshops. In addition to these HEA activities, RHESSI also supported other teacher professional development activities in FY09. Dr. Bryan Mendez presented the RHESSI magnetism and solar-flare teacher's guide and/or general magnetism activities at several other week-long teacher professional development workshops put on by other organizations: National Science Teachers Association (NSTA), 2009; California Science Teachers Association (CSTA), 2009; the University of Colorado's Laboratory for Atmospheric and Space Physics (LASP)'s week-long NASA science workshop in July, 2009; and at the Oakland, CA, school district's training on math and science (using the Lawrence Hall of Science FOSS curriculum and kits), where space weather was used as a 'storyboard' for the context of the physical science being taught to these elementary school teachers. As an additional offshoot of this partnership, the LHS FOSS personnel have since used the NASA-funded magnetism lessons in other professional development opportunities that they have participated in.

4.1.2 Goddard

RHESSI / STEREO: Podcasting and Social Media

The Sun-Earth Day program coordinates scientific and educational resources of NASA's heliophysics missions to tell a compelling and coherent story of phenomena within the heliosphere. Our web-based resources, webcasts and podcasts have been accessed over 200 million times since SED began in 2000.

Ongoing communication between Heliophysics scientists, educators and the general public is greatly enhanced by through Sun-Earth Day's growing social network (i.e. Facebook, Twitter, YouTube). Integrating RHESSI and STEREO information into these networks will strengthen the relationship we have with our existing community and broaden the reach of our E/PO programs.

The SED program would enhance the presence of RHESSI and its relation to STEREO through the development of a series of dedicated podcasts focused on the latest RHESSI and STEREO science and education information. The series would be promoted through existing SED resources and our network of scientists, educators, students and museums. Content for each podcast would include a wide range of topics including: scientist interviews, mission highlights, featured activities, website information, multimedia resources, etc. Links to each

podcast would be made available on the SED and mission websites. The podcast series would also be enhanced through the development of a ‘Primary Source’ activity designed to show users how to integrate each podcast with existing mission videos, image galleries, the Space Weather Media Viewer and the Space Weather Action Center program. Teachers can also use the videos and descriptive podcasts to enhance their curriculum, especially when teaching about our Sun's connection to the polar environment.

Sample ‘Primary Resource’ activity: http://sunearthday.nasa.gov/polarsunrise/index.php

4.2 RHESSI Legacy Mission Archive Plan

4.2.1 Introduction

Normal RHESSI operations are largely autonomous, with a routine daily command upload containing the telemetry schedule and occasional adjustments to instrument parameters. Except during eclipse periods, passages through the South Atlantic Anomaly, and an annual Crab Nebula observing campaign, RHESSI observes the full Sun continuously.

The primary science data are returned in event data packets whose contents include the time, energy and detector-segment identification for each detected photon. Aspect data are provided with sufficient time resolution that the instantaneous aspect associated with each detected event can be inferred. Monitor Rates with lower time resolution are also available to provide an overview of detector performance.

Data acquisition averages about 2 GBytes per day and is based on a store-and-dump system using a 4 Gbyte on-board memory. There are typically ~11 prescheduled downlink passes per day divided between the Berkeley Ground Station (BGS) and NASA Wallops Ground Station (WGS) with additional telemetry support provided by ground stations at Merritt Island (MILA), Weilheim, Germany, and Santiago, Chile (AGO).

Because the RHESSI data is photon-based, analysts can (iteratively) choose the optimum time, spectral and spatial resolution and coverage best suited to his/her specific science objectives and the flare(s). Such decisions can therefore be made during the analysis phase, as opposed to the implementation or operations phase of the mission. This provides a powerful degree of flexibility whose value has been proven over the years. Preserving this flexibility is a primary driver for the RHESSI analysis software and data strategy.

4.2.2 Current RHESSI Data Archive, Software and Documentation

4.2.2.1 RHESSI Data Archive

The current RHESSI data archive contains the full Level-0 telemetry data, the RHESSI flare list, and a number of catalog or quicklook data products (QLP) including mission-long light curves, flare spectra and images, and summaries of housekeeping data. The full archive (~6 TB as of March 2010) resides on servers at SSL and is automatically mirrored at GSFC and the HESSI Experimental Data Center (HEDC) at FHNW, Windisch, Switzerland. It is online and accessible by anyone with an Internet connection. The on-line archive, including metadata, quicklook products and engineering data, is updated automatically, typically within an hour of receipt at the MOC by converting the received telemetry to FITS files and adding it to the online dataset where it is available for scientific analysis.

The Level-0 data files contain the full raw telemetry data in packed time-ordered format. All of the quicklook product generation and detailed analyses of RHESSI data start with the Level-0 files. These files are in FITS format and contain science data ('photon-tagged events' that encode the detector ID, arrival time, and energy for each detector count), monitor rates, solar aspect data and housekeeping data . Even though these files are in standard FITS format, they are meaningful only through the RHESSI SSW software due to the complicated unpacking algorithms. Calibration information needed to interpret these data is distributed with and accessed by the analysis software. The entire Level-0 database is currently being backed up into a deep archive at the NSSDC with a latency of a few months. As of February 2010, it contains data through November 2009.

The QLP includes a flare list containing the time, duration, size, location, and other parameters and flags for the >50,000 events automatically identified in the RHESSI data. The full flare list is available in the archive (and viewable through a browser) as one large text file. In addition, monthly flare list files are stored in FITS format, as well as text files for easy direct viewing. The RHESSI software reads the FITS files, automatically merging the monthly files, and provides options for selecting analysis time intervals based on flare parameters.

The quick-look products (QLP) allow the RHESSI observations to be surveyed. Using the same software used for higher-level analysis, they are created automatically from the Level-0 data both as FITS files and browser-viewable image formats such as GIF, PNG, or text files.

The FITS QLPs include daily observing summary data files from which analysts can quickly generate 4-second plots of light curves in 9 standard energy bands, spacecraft ephemeris, pointing and modulation variance. For most flares, the QLP also include representative spectra and images that are intended as a starting point for most analyses. (Detailed analysis of a flare is usually done using the Level-0 data, where the user can select the times, energies, detectors, etc. that are best suited to the scientific objectives and the event under study.) The prepared plots can be viewed directly by accessing the archive metadata directories, or more easily through the versatile RHESSI Quick-

Look Browser at http://sprg.ssl.berkeley.edu/~tohban/browser/ which allows users to display more than 20 different products (including light curves, images, spectra, monitor rates and comparisons with GOES, WIND/WAVES and WIND/3DP).

In addition, RHESSI housekeeping data for the entire mission are available in the archive and can be accessed at http://hessi.ssl.berkeley.edu/hessidata/metadata/hsi_1day_sohdata/.

Text files and GIF plots provide a record of the average daily values for ~100 state-of-health parameters including spacecraft bus voltages and currents, imager aspect sensor parameters, spectrometer cryocooler power and temperature, and more.

Access to the data archive is almost transparent. Users located at a site hosting the full data archive (Goddard, Berkeley, or FHNW) share the data directories from a local file server. Remote users set a feature in the software to enable network searching and copying of files from an archive to their own computer. In either case, the software automatically determines the files needed for the selected time interval and after either sharing or copying them, reads them and retrieves the requested data for processing.

Another, separate, extensive source of quick-look products is an archive at the Swiss-funded HESSI Experimental Data Center at FHNW in Windisch, Switzerland (formerly at ETHZ in Zurich) - http://www.hedc.ethz.ch/ . It provides a large array of pre-processed images, spectra, spectrograms, and more for each RHESSI flare.

4.2.2.2 Software

Almost all the RHESSI software package (Schwartz et al. 2002) is written in Interactive Data Language (IDL licensed from ITT Visual Data Solutions). It contains all procedures necessary to read and unpack the FITS data files, prepare and plot light curves, reconstruct images, and accumulate, display, and analyze spectra. Analysis procedures can be invoked from the IDL command line, from user-generated scripts building on these commands, or from a graphical user interface (GUI) that forms a user-friendly shell around the basic analysis routines. The software is fully compatible with both UNIX-like (including Mac OS X) and Windows operating systems and is freely available as part of the Solar Software (SSW) tree.

The RHESSI data analysis software is a robust object-oriented system that allows any analyst with access to Level-0 files, calibration data, and the QLPs to generate and analyze RHESSI lightcurves, spectra, and images. Higher level capabilities include generating image cubes and movies of images at multiple time and energy intervals, background subtraction, feature-based imaging spectroscopy, and performing joint analysis of many different observations of the same events by other observatories. The software can be downloaded to any user's computer as part of the Solar Software (SSW) installation following instructions provided on the RHESSI web site. The only requirement is that the user has a license for IDL Version 5.6 or higher.

4.2.2.3 Documentation and Support

Extensive documentation describing the mission, instrumentation, analysis techniques, software, and data access can be found via a single RHESSI web site: http://hesperia.gsfc.nasa.gov/rhessidatacenter/. Support personnel at SSL and GSFC are also available to provide guidance as needed in using the software and interpreting the results.

The extensive online RHESSI documentation provides both background and explanatory material on the RHESSI mission, as well as instructions for almost every aspect of the software, from installation through use of the objects and the GUI. Detailed descriptions of every data product and warnings about misinterpreting data are available. There are 'First Steps' instructions for imaging and spectroscopy to guide users through sample GUI sessions and explanations of the use of the objects. A software FAQ is available to provide solutions to common questions or problems.

There is a dedicated email address (hessibugs@hesperia.gsfc.nasa.gov), monitored by one of the team members, for RHESSI software bug reports and questions. Queries are answered promptly either by the monitor or by core members of the RHESSI group who can be called upon as needed to address more specialized issues. All bug reports and their solutions are archived for user access.

4.2.3 Plans for the RHESSI Legacy Archive

4.2.3.1 Introduction

In general, the data products, software and documentation discussed above will be incorporated into the legacy archive. This section emphasizes those tasks related to adapting those data sets to make them effective with a

reduced (or eliminated) level of support from the instrument team, and includes a discussion of additional archive material not discussed above. In broad terms, there are four classes of data products to be provided in the legacy archive:

1. Catalog data, providing basic Level-1 data products with predetermined parameterization to provide an overview of the data and to support relatively undemanding applications;
2. Level-0 plus documented software to provide maximum analysis flexibility;
3. Calibrated visibility data to provide considerable flexibility in time and energy resolution for flare analyses using either a simplified subset of existing software or external analysis packages;
4. Secondary databases to support exploitation of the high-precision solar radius measurements and non-solar analyses.

4.2.3.2 Data Products

Catalog Data

The catalog data products serve the needs of those requiring a convenient overview of the data and basic X-ray data products (light curves, representative images, and spectra, etc.). The catalog data to be archived for post-mission use are identical in form and content to that described in the preceding section. During the Resident Archive phase, the number of quick look images will be increased to reduce the need for post-mission image reconstruction. Automated tools for creating such products exist.

Level-0 Data

To meet the needs of solar and non-solar analyses without compromising the potential of the data, the Level-0 data as described in the preceding section will be made part of the resident and permanent archives, along with the corresponding analysis tools and documentation.

Visibility Data

As discussed above, a key driver of the RHESSI analysis approach has been to maintain the ability of the user to flexibly choose the time, spatial, and energy resolution and range that best matches their scientific objectives and events under study. To achieve this, however, it is necessary for users to start from Level-0 data and use the RHESSI-specific IDL software package. While this continues to be effective, it may become more problematic without the occasional one-on-one interaction with experienced users. For the long-term therefore, it is desirable to identify a way by which most of the flexibility can be maintained without necessarily resorting to the Level-0 data.

Visibilities provide a natural way to accomplish this. A RHESSI visibility is a fully calibrated measurement of a specific Fourier component of the source spatial distribution for a given time interval and (count) energy bin. In radio parlance, each visibility corresponds to a single uv point. Such visibilities are a direct output of RHESSI's time-modulated measurements of X-ray flux. While RHESSI's 'normal' imaging algorithms bypass the explicit calculation of visibilities, within the last two years, the object-oriented software to convert RHESSI's photon-based data to calibrated visibilities has been incorporated into the RHESSI software package and an increasing fraction of papers now use visibility-based analyses. Furthermore, some capabilities, such as the generation of electron-images, can only be generated through visibilities.

While making some compromises in time and/or energy resolution, the use of visibilities has several distinct advantages.

- Visibilities are an inherently compact representation of the RHESSI data, preserving its key information content in a form that is typically ~2 orders of magnitude more compact than photon-based data.
- Unlike reconstructed images, visibilities are a *linear* representation of the data so they can be combined across different time/energy ranges to meet the user's needs.
- For each detected energy range, visibilities are fully calibrated, thus relieving the user of instrument-specific calibration tasks.
- Visibilities provide a more robust method of determining accurate source sizes as compared to inspection of reconstructed images.
- Measured visibilities include well-determined statistical errors whose propagation supports quantitative assessment of the significance of derived results.
- Calibrated X-ray visibilities have the identical significance as visibilities obtained from radio interferometers. Thus, a set of X-ray visibilities can be manipulated and converted to an image using any of several existing radio interferometer analysis packages, *independent of RHESSI-specific software.*

These considerations suggest that, in addition to the catalog and Level-0 data products discussed above, the inclusion of an extensive set of calibrated flare X-ray visibility data would provide a flexible option to meet the needs of users well into the future.

To do so, the following tasks remain to be accomplished:

- While the basic software for visibility calculation has been implemented, there are several important areas in which it needs to be refined.
- Automated algorithms need to be developed to optimally choose statistically significant time and energy intervals within which to calculate visibilities. Such algorithms are currently under development for other missions (e.g. Solar Orbiter) and can be re-parameterized for the present purpose.
- Scripts need to be developed and executed to apply these algorithms to the mission-long RHESSI data set.
- The optimum data format for the calculated visibilities needs to be identified to support long-term use and to ensure compatibility with radio software packages.
- More extensive documentation needs to be developed for use by unsupported users in the Resident and/or Permanent archive phases.

4.2.4 Other Databases

The additional databases described in this section have the common feature that the data are distributed throughout the multi-terabyte Level-0 database. As a result, it is desirable to extract and process the relevant material into compact, standalone databases for subsequent analysis.

4.2.4.1 Solar Radius Data

In addition to providing essential pitch and yaw aspect data for X-ray image reconstruction, the solar aspect system (SAS) data constitute a unique database of highly precise measurements of solar radii (Fivian et al. 2005) with applications to fundamental solar properties such as solar oblateness and p-modes,. The dataset comprises ~100 radius measurements per second (totaling $>10^{10}$ measurements to date), each with a statistical error of a few milli-arcseconds.

SAS data require elaborate analyses to remove diverse systematic effects in order to obtain their inherent precision. As a result, these data benefit from the creation of secondary databases, both to isolate the SAS data set itself and to reflect the application of internally derived calibration parameters. Although a preliminary version of such a database exists, for the legacy archive, it will need to be finalized and fully documented, a task that will require ~ 1 man-year.

4.2.4.2 Radiation Studies

Mission-long examination of nuclear radiation data is useful for studies of galactic Al^{26}, galactic positron annihilation, novae, and quiet-Sun 2.2 MeV neutron-capture-line emission. As the mission progresses a database of accumulated 1-minute spectra from the rear detector segments is being amassed and will be added to the Permanent Archive. Documentation will be generated during the transition to the Resident Archive Phase.

4.2.4.3 Terrestrial Gamma-Ray Flashes

A catalog of transient events identified by an automated TGF triggering algorithm is being assembled as the mission progresses. During the Resident Archive phase, this will be finalized and documented for use as part of the Permanent Archive.

4.2.5 Analysis Tools for Level-0 data

The basis for all Legacy Archive analysis tools is the IDL-based, SSW-distributed software that has been routinely used during the mission for the creation and interpretation of scientific data products. To maintain the integrity of the software within the dynamic SSW environment we will archive a snapshot of all the elements of the SSW tree necessary for RHESSI analysis, specifically the GEN, HESSI, X_RAY, and SPEX branches. This will ensure that the software that was working at the end of mission will continue to work into the future.

With successive cycles of progressive radiation damage and annealing, the RHESSI detector response has changed during the course of the mission. To accommodate this, detector response parameters in the SSW distribution have been periodically updated so that, transparent to the user, the appropriate time-dependent calibration parameters are applied for each analysis. In preparation of the legacy archive, it will be necessary to ensure that this calibration has been updated as required to cover the full mission

4.2.6 Documentation

While an extensive range of documentation is available via the RHESSI website, it needs to be carefully reviewed so that it can effectively serve its purpose during the Resident and Permanent Archive phases with reduced (or absent) one-on-one support. Specifically, obsolete or conflicting material needs to be identified and updated or removed, perceived gaps need to be identified and a robust stand-alone guide to the material generated. While on-going at a low level, this task will be completed during the Resident archive phase, requiring an estimated 2-4 months of effort by a combination of experienced RHESSI personnel. Additional emphasis will be placed on introductory material, indexing, and consolidating distributed information to provide a mission-long overview and time-ordered log of RHESSI performance.

4.2.7 Distribution

During the year after the end of the mission, RHESSI data products will continue to be accessible from servers at SSL and GSFC (and possibly through the Swiss-funded mirror site at FHNW). The archive will then be transitioned to the Resident Archive at the Solar Data Analysis Center (SDAC) at Goddard. The Legacy Archive will be hosted by the National Space Science Data Center (NSSDC) at Goddard.

Access of RHESSI data through the VSO involves three approaches. The first is to include the Catalog data into the VSO. This will make it possible on one hand, to display quick-look products in VSO query results, and on the other, to download pre-calculated images or image cubes for comparison with data sets from other instruments. This requires no RHESSI-specific software.

The second approach is to implement event-based queries, i.e. queries based on the flare list and the observing summary in addition to queries based on a time range. This means that the RHESSI archive can be searched, for example, for flares of specific characteristics such as size, duration, or location on the limb.

The third approach is to provide an indexed database of flare visibilities, a subset of which can be identified and provided in response to user time, energy, location or other criteria. These can be manipulated and/or converted to images at the user's institution using either a simplified subset of IDL software or by external radio interferometric packages such as Miriad.

To allow correct inclusion of the RHESSI data into the VSO, the Catalog data will be annotated in the FITS headers with keywords defined by the SPASE consortium. Adopting SPASE keywords will guarantee that SPASE data analysis programs can use RHESSI Catalog data. The visibility data will also be described by SPASE-compatible keywords. The Level-0 database, however, does not need to be SPASE annotated, as it requires the RHESSI-specific software to generate science ready products.

4.2.8 Schedule

Estimates of the effort required to go from the end of mission to complete documentation and delivery of the legacy archive are as follows: Catalog and level-0 data preparation: 0.1 FTE; visibility data software development, validation and database generation 2 FTE, solar radius data 1 FTE; radiation studies: 0.2 FTE; TGF database: 0.2 FTE; analysis tools, 0.2 FTE; documentation 0.4 FTE, distribution, 0.5 FTE; for a total of 4 to 5 FTE. These tasks should be completed within an elapsed time of ~2 years from the end of mission using an appropriate mix of experienced RHESSI personnel.

4.2.9 References

Fivian, M. D., Hudson, H. S. and Lin., R. P., 2005 in *Proc 11th European Solar Physics Meeting*, ESA SP- 600, 41.
Lin, R. P. et al., 2002, Solar Physics, 210, 3.
Schwartz, R. S. et al., 2002, Solar Physics, 210, 165.

5 ACRONYM LIST

AAS	American Astronomical Society
ACE	Advanced Composition Explorer
ACS	Attitude Control System
AESP	Aerospace Education Services Program
AGO	Santiago ground station
AGU	American Geophysical Union
AIM	Aeronomy of Ice in the Mesosphere
AISES	American Indian Science and Engineer Society
ASIM	Atmosphere-Space Interactions Monitor
ATS	Absolute Time Sequence
AU	Astronomical Unit
BATSE	Burst and Transient Source Experiment on CGRO
BGO	Bismuth Germinate used as a scintillation detector
BGS	Berkeley Ground Station
BPSK	Binary Phase Shift Keying
CAST	CERN Axion Solar Telescope
CCD	Charge Coupled Device
CD-ROM	Compact Disk – Read Only Memory
CDS	Coronal Diagnostic Spectrometer on SOHO
CERN	European Organization for Nuclear Research
CHIPS	Cosmic Hot Interstellar Plasma Spectrometer
CGRO	Compton Gamma Ray Observatory
CINEMA	Cubesat for Ion, Neutral, Electron, & Magnetic fields
CLI	Command Line Interface
CME	Coronal Mass Ejection
COMPTEL	Compton Telescope on CGRO
COR-1	Inner Coronagraph of STEREO SECCHI instrument
COR-2	Outer Coronagraph of STEREO SECCHI instrument
COSPAR	COmmittee on SPAce Research
CP	Charge conjugation/Parity
CSE@SSL	Center for Science Education at Space Sciences Laboratory
CSTA	California Science Teachers Association
DEM	Differential Emission Measure
DLR	Weilheim ground station
EGRET	Energetic Gamma Ray Experiment Telescope on CGRO
ERC	Educator Resource Center
EEPROM	Electrically Erasable Programmable Read-Only Memory
EIT	Extreme Ultraviolet Imaging Telescope on SOHO
EIS	EUV imaging spectrograph on Hinode
E/PO	Education and Public Outreach
ETH	Eidgenossische Technische Hochschule, Zurich, Switzerland
ETHZ	Eidgenössische Technische Hochschule (Zentrum)
EUV	Extreme UltraViolet
EUVI	Extreme UltraViolet Imager on STEREO
EVA	Extra-Vehicular Activity
FAST	Fast Auroral SnapshoT
FAQ	Frequently Asked Questions
FDC	Flight Dynamics Center
Fermi	Fermi Gamma-ray Space Telescope (formerly GLAST)
FFT	Fast Fourier Transform
FHNW	Fachhochschule Nordwestschweiz
FIP	First Ionization Potential
Firefly	NASA microsatellite for studying TGFs
FITS	Flexible Image Transport System

FORMOSAT-2	Earth Observation Satellite
FOT	Flight Operations Team
FoV	Field of View
FTE	Full time Equivalent
FWHM	Full Width at Half Maximum
GB	Gigabytes
GBM	Gamma-ray Burst Monitor on Fermi
GDS	Ground Data System
Ge	Germanium
GeD	Germanium Detector
GEMS	Great Explorations in Math and Science
GEONS	Geomagnetic Event Observation Network by Students
GIF	Graphics Interchange Format
GLAST	Gamma-ray Large Area Space Telescope (now Fermi)
GOES	Geostationary Operational Environmental Satellite
GRB	Gamma Ray Burst
GRS	Gamma Ray Spectrometer
GSFC	Goddard Space Flight Center
G/T	Antenna gain to noise temperature ratio
GUI	Graphical User Interface
HD	Heliophysics Division
HEAD	High Energy Astrophysics Division
HEDC	HESSI European Data Center
HEPAD	High Energy Proton and Alpha Particle Detector on GOES
HGO	Heliophysics Great Observatory
Hinode	Japanese solar satellite - formerly Solar-B
HMI	Helioseismic and Magnetic Imager on SDO
HP	Heliophysics
HST	Hubble Space Telescope
HXR	Hard X-ray
HXT	Hard X-ray Telescope on Yohkoh
IDL	Interactive Data Language
IDPU	Instrument Data Processing Unit
IGES	Institute for Global Environmental Strategies
IMPACT	In-situ Measurements of Particles and CME Transients on STEREO
IPM	Interplanetary Medium
ISUAL	Imager of Sprites and Upper Atmospheric Lightnings on FORMOSAT-2
ITOS	Integrated Test and Operations System
KSC	Kennedy Space Center
LASCO	The Large Angle and Spectrometric Coronagraph on SOHO
LAT	Large Area Telescope on Fermi
LHCP	Left-Handed Circular Polarization
LHS	Lawrence Hall of Science
LSEP	Large SEP event
mas	milli-arcsecond
MB	Megabytes
MDI	Michelson Doppler Imager on SOHO
MHD	Magnetohydrodynamics
MILA	Merritt Island ground station
MOC	Mission Operations Center
MOU	Memorandum of Understanding
MPS	Mission Planning System
NaI	Sodium Iodide used as a scintillation particle detector
NASA	National Aeronautics and Space Administration
NSSDC	National Space Science Data Center

NSTA	National Science Teacher Association
NuSTAR	Nuclear Spectroscopic Telescope Array
OCA	Orbital Carrier Aircraft
OIG	Orbital Information Group
PD	Professional Development
PMTRAS	Photomultiplier Tube Roll Angle System
PNG	Portable Network Graphics
PSLA	Project Service Level Agreement
QLP	Quick Look Product
RAD6000	Radiation-hardened single board computer used on spacecraft
RAS	Roll Angle System
RF	Radio Frequency
RHCP	Right-Handed Circular Polarization
RHESSI	Reuven **R**amaty **H**igh **E**nergy **S**olar **S**pectroscopic **I**mager
RMC	Rotating Modulation Collimator
SAA	South Atlantic Anomaly
SACNAS	Society for Advancement of Chicanos and Native Americans in Science
SAMPEX	Solar Anomalous and Magnetospheric Particle Explorer
SAS	Solar Aspect System
SatTrack	Satellite Tracking software
SDAC	Solar Data Analysis Center
SDO	Solar Dynamics Observatory
SECCHI	Sun Earth Connection Coronal and Heliospheric Investigation on STEREO
SECEF	Sun Earth Connection Education Forum
SEGway	Science Education Gateway
SEP	Solar Energetic Particles
SEPT	Solar Electron Proton Telescope on STEREO / IMPACT
SERS	Spacecraft Emergency Response System
SHH	Soft, Hard, Harder – spectral evolution
SHS	Soft, Hard, Soft – spectral evolution
SMEX	NASA's Small Explorer Program
SMM	Solar Maximum Mission
SOC	Science Operations Center
SOH	State-Of-Health
SOHO	Solar and Heliophysics Observatory
SOT	Solar Optical Telescope on Hinode
SPASE	Space Physics Archive Search and Extract
SPD	Solar Physics Division
SSL	Space Sciences Laboratory (University of California, Berkeley)
SSR	Solid State Recorder
STE	Suprathermal Electron Telescope on STEREO / IMPACT
STEREO	Solar TErestrial RElations Observatory
STIX	Spectrometer Telescope for Imaging X-rays
SSW	SolarSoftware
STEM	Science, Technology, Engineering, and Math
SXI	Soft X-ray Imager
TARANIS	Tool for the Analysis of RAdiations from lightNIngs and Sprites, European Satellite Project
TB	Terabytes
TGF	Terrestrial Gamma-ray Flash
THEMIS	Time History of Events and Macroscale Interactions during Substorms
TRACE	Transition Region and Coronal Explorer
UCB	University of California at Berkeley
UT	Universal Time
VCn	Virtual Channel n
VSO	Virtual Solar Observatory
VxWorks	A real-time operating system

WGS	Wallops Ground Station
WISE	Wide Field Infrared Survey Explorer
XRT	X-Ray Telescope on Hinode
Yohkoh	Japanese Solar Observatory Satellite